CHAPTER 2

LITERATURE REVIEW

2.1 Electronic properties of semiconductors

Semiconductor is a material whose electrical conductivity is midway between that of an good conductor and a good insulator; a type of material having a lower energy valence band that is nearly completely filled with electrons and a higher energy conduction band that is nearly completely empty of electrons, with a modest energy gap between the two bands; pure materials usually exhibit electrical conductivity that increases with temperature because of an increase in the number of charge carriers being promoted to the conduction band.

2.1.1 Band structure [1-2, 11]

Energy bands consisting of a large number of closely spaced energy levels exist in crystalline materials. The bands can be thought of as the collection of the individual energy levels of electrons surrounding each atom. The wave functions of the individual electrons, however, overlap with those of electrons which is confined to neighboring atoms. Pauli exclusions principle does not allow the electron energy levels to be the same so that one obtains a set of closely spaced energy levels, forming an energy band. The energy band model is crucial to any detailed treatment of semiconductor devices. It provides the framework needed to understand the concept of an energy band gap and that of conduction in an almost filled band as described by the empty states.

In semiconductors and insulators, electrons are confined to a number of bands of energy, and forbidden from other regions. The term "band gap" refers to the energy difference between the top of the valence band and the bottom of the conduction band; electrons are able to jump from one band to another. In order for an electron to jump from a valence band to a conduction band, it requires a specific minimum amount of energy for the transition. The required energy differs with different materials. Electrons can gain enough energy to jump to the conduction band by absorbing either a phonon (heat) or a photon (light).

A material with a small but nonzero band gap which behaves as an insulator at absolute zero but allows thermal excitation of electrons into its conduction band at temperatures which are below its melting point is referred to as a semiconductor. A material with a large band gap is called an insulator. In conductors, the valence and conduction bands may overlap, so they may not have a band gap.

The conductivity of intrinsic semiconductors is strongly dependent on the band gap. The only available carriers for conduction are the electrons which have enough thermal energy to be excited across the band gap.

The distinction between semiconductors and insulators is a matter of convention. One approach is to think of semiconductors as a type of insulator with a narrow band gap. Insulators with a larger band gap, usually greater than 3 eV are not considered semiconductors and generally do not exhibit semi-conductive behaviour under practical conditions. Electron mobility also plays a role in determining a material's informal classification.

The band gap energy of semiconductors tends to decrease with increasing temperature. The amplitude of atomic vibrations increase, when temperature increase, leading to larger interatomic spacing. The interaction between the lattice phonons and the free electrons and holes will also affect the band gap to a smaller extent. The relationship between band gap energy and temperature can be described by Varshni's empirical expression, [25]

$$E_g(T) = E_g(0) - \frac{\alpha T^2}{(T+\beta)} \tag{2.1}$$

where $E_g(0)$, α and β are material constants

In a regular semiconductor crystal, the band gap is fixed owing to continuous energy states. In a quantum dot crystal, the band gap is size dependent and can be altered to produce a range of energies between the valence band and conduction band. It is also known as quantum confinement effect.

Band gaps also depend on pressure. Band gaps can be either direct or indirect, depending on the electronic band structure.

The electrical conductivity of semiconductors ranges from about 10^3 to 10^{-9} Ω^{-1} cm^{-1}, as compared with a maximum conductivity of 10^7 for good conductors and a minimum conductivity of 10^{-17} Ω^{-1} cm^{-1} for good insulators.

The electric current is usually due only to the motion of electrons, although under some conditions, such as very high temperatures, the motion of ions may be important. The basic distinction between conduction in metals and in semiconductors is made by considering the energy bands occupied by the conduction electrons.

At absolute zero temperature, the electrons occupy the lowest possible energy levels, with the restriction that at most two electrons with opposite spin may be in the same energy level. In semiconductors and insulators, there are just enough electrons to fill completely a number of energy bands, leaving the rest of the energy bands empty. The highest filled energy band is called the valence band. The next higher band, which is empty at absolute zero temperature, is called the conduction band. The conduction band is separated from the valence band by an energy gap, which is an important characteristic of the semiconductor. In metals, the highest energy band that is occupied by the electrons is only partially filled. This condition exists either because the number of electrons is not just right to fill an integral number of energy bands or because the highest occupied energy band overlaps the next higher band without an intervening energy gap. The electrons in a partially filled band may acquire a small amount of energy from an applied electric field by going to the higher levels in the same band. The electrons are accelerated in a direction opposite to the field and thereby constitute an electric current. In semiconductors and insulators, the electrons are found only in completely filled bands, at low temperatures. In order to increase the energy of the electrons, it is necessary to raise electrons from the valence band to the conduction band across the energy gap. The electric fields normally encountered are not large enough to accomplish this with appreciable probability. At sufficiently high temperatures, depending on the magnitude of the energy gap, a significant number of valence electrons gain enough energy thermally to be raised to the conduction band. These electrons in an unfilled band can easily participate in conduction. Furthermore, there is now a corresponding number of vacancies in the electron population of the valence band. These vacancies, or holes as they are called, have the effect of carriers of positive charge, by means of which the valence band makes a contribution to the conduction of the crystal.

The type of charge carrier, electrons or holes, that is in largest concentration in a material is sometimes called the majority carrier and the type in smallest concentration the minority carrier. The majority carriers are primarily responsible for the conduction properties of the material. Although the minority carriers play a minor role in electrical conductivity, they can be important in rectification and transistor actions in a semiconductor.

Many materials are capable of emitting visible luminescence when subjected to some form of excitation such as UV light (photoluminescence), heat (thermoluminescence), chemical reactions (chemiluminescence), and electric fields (electroluminescence). There are two pre-requisites for luminescence: (1) the luminescent material must have a semiconductor structure with a nonzero band gap E_g (e.g. metals do not luminescence since they have no band gap); (2) energy must be imparted to this material before luminescence can take place. The mechanism of photoluminescence in semiconductors is schematically illustrated in Figure 8, which plots the E-k diagrams for a direct band gap material (left) and an indirect gap material (right), where E and k are respectively the kinetic energy and wave vector (or "momentum vector") of the electron or hole ($E = \hbar^2 k^2 / 2m^*$; where $\hbar = h / 2\pi$ is the Planck constant h divided by 2, and m* is the electron or hole effective mass). The direct and indirect gap materials are distinguished by their relative positions of the conduction band minimum and the valence band maximum in the Brillouin Zone (the volume of k space containing all the values of k up to π/a where a is the unit lattice cell dimension). In a direct gap material, both the conduction band minimum and the valence band maximum occur at the zone center (k=0). In an indirect gap material, however, the conduction band minimum does not occur at zone center, but rather at some other values of k which is usually at the zone edge or close to it.

Upon absorption of an UV or visible photon with an energy $\hbar\omega_{exc}$ exceeding the band gap E_g (the gap in energy between the valence band and the conduction band) of the material, an electron-hole pair is created and the electron (hole) is excited to states high up in the conduction (valence) band. During a photon absorption process in semiconductors, we must conserve both energy and momentum. In a direct band gap material, the conduction band minimum and the valence band maximum have the same k (i.e., $\hbar\vec{k}_i = \hbar\vec{k}_f$, where $\vec{k}_i$ and $\vec{k}_f$ are respectively the wave vectors of the initial and final electron states; this implies that the electron wave vector should not change significantly during a photon absorption process), conservation of momentum is guaranteed for the photoexcitation of the electron which only involves a UV or visible photon: $\hbar\vec{k}_i + \hbar\vec{k}_{photon} \approx \hbar\vec{k}_i = \hbar\vec{k}_f$ since $\vec{k}_{photon}$, the wave vector of the absorbed photon (which is in the order of $2\pi/\lambda \sim 10^5$ cm^{-1}), is negligible compared to the electron wave vector (which is related to the size of the Brillouin zone $\pi/a \sim 10^8$ cm^{-1}, where the unit cell dimension a is in the order of a few angstroms). This implies that in a direct band gap material, the electron wave vector does not change significantly during a photon absorption process. We therefore represent photon absorption processes by vertical arrows in the diagrams.

In contrast, for an indirect band gap material of which the conduction band minimum and the valence band maximum have different k values, conservation of momentum implies that the photon absorption process must be assisted by either absorbing or emitting a phonon (a quantum of lattice vibration), because the electron wave vector must change significantly in jumping from the valence band in state

$(E_i, \vec{k}_i)$ to a state $(E_f, \vec{k}_f)$ in the conduction band, and the absorption of a photon alone cannot provide the required momentum change since $\left|\vec{k}_{photon}\right| << \left|\vec{k}_i - \vec{k}_f\right|$.

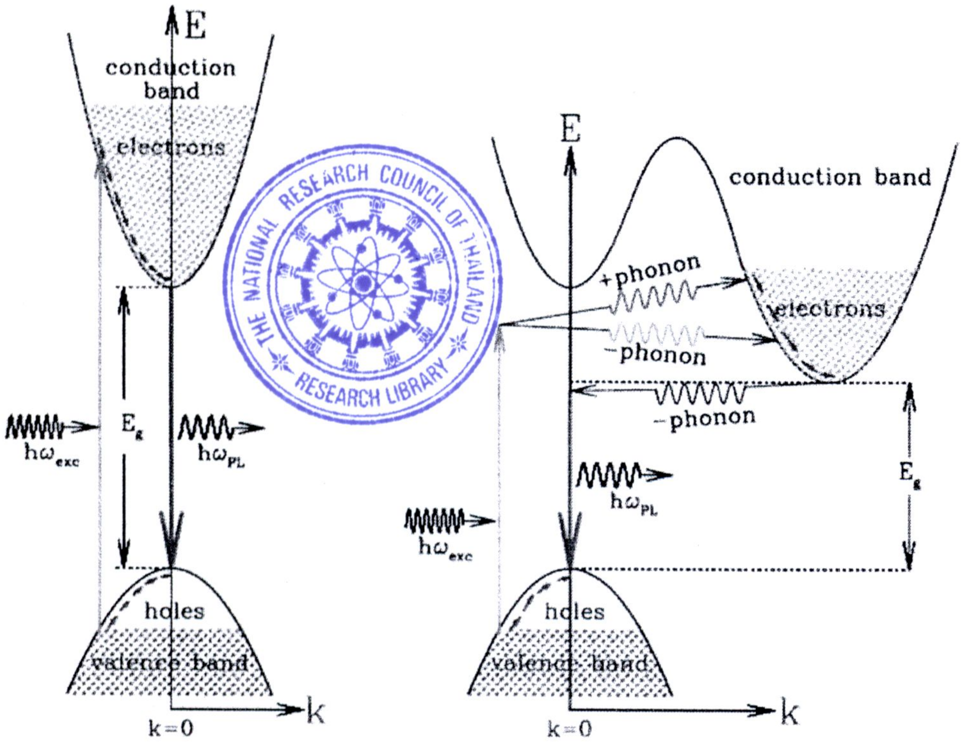

direct-gap materials

indirect-gap materials

Figure 2.1 Schematic band diagrams for the photoluminescence processes in a direct gap material (left) and an indirect gap material (right)

The excited electron and hole will not remain in their initial excited states for very long; instead, they will relax very rapidly (~ 10^{-13} s) [1] to the lowest energy states within their respective bands by emitting phonons. When the electron (hole) finally arrives at the bottom (top) of the conduction (valence) band, the electron-hole pair can recombine radiatively with the emission of a photon (luminescence), or nonradiatively by transferring the electron's energy to impurities or defects in the material or dangling bonds at the surface.

The National Research Council of Thailand
Research Library
Date....22 NOV 2012....
Record No. ....E46223....
Call No. ....

Just like the photon absorption process discussed above, the electron-hole recombination in a direct band gap material does not involve any phonons since there is no need for momentum change for the electron. In contrast, in an indirect gap material, the excited electron located in the conduction band needs to undergo a change in momentum state before it can recombine with a hole in the valence band; conservation of momentum demands that the electron-hole recombination must be accompanied by the emission of a phonon, since it is not possible to make this recombination by the emission of a photon alone. Compared to the photon absorption process in an indirect gap material for which conservation of momentum can be fulfilled by either absorption or emission of a phonon, in the electron-hole recombination process phonon absorption becomes negligible, whereas phonon emission becomes the dominant momentum conservation mediator because (1) the number of phonons available for absorption is small and is rapidly decreasing at lower temperatures, whereas the emission of phonons by electrons which are already at a high-energy state is very probable; and (2) an optical transition assisted by phonon emission occurs at a lower photon energy $E_g - h\nu_{phonon}$ than the gap energy, whereas phonon absorption results in a higher photon energy of at least $E_g + h\nu_{phonon}$, which can be more readily re-absorbed by the semiconductor nanoparticle. But we note that the energy of a phonon ($h\nu_{phonon}$) is just in the order of ~ 0.01 eV, much smaller than the energy of the electron-hole recombination luminescence photon. Also because prior to the recombination, the electrons and holes respectively accumulate at the bottom of the conduction band and the top of the valence band, the energy separation between the electrons and the holes approximately equals to the energy of the band gap. Therefore, the luminescence emitted by both types of semiconductors occurs at an energy close to the band gap (E_g).

The PL efficiency is determined by the competition between radiative and nonradiative recombination. For an indirect gap material, the PL process, which requires a change in both energy and momentum for the excited electron and hence involves both a photon and a phonon, is a second-order process with a long radiative lifetime (~ 10^{-5} -10^{-3} s) [8,9], and therefore a relatively small efficiency because of the competition with nonradiative combination. In contrast, in a direct gap material, the emission of a PL photon does not need the assistance of a phonon to conserve momentum. Therefore, the PL process in a direct gap material is a first-order process with a much shorter radiative lifetime (~ 10^{-9} -10^{-8} s) and a much higher PL efficiency in comparison with an indirect gap material.

However, for particles in the nanometer size domain, we would expect substantial changes in both the efficiency and the peak energy of the photoluminescence due to the quantum confinement effect. This can be understood in terms of the Heisenberg uncertainty principle. Unlike in bulk materials the electrons and holes are free to move within their respective bands in all three directions, in nanoparticles the electrons and holes are spatially confined and hence their motion is quantized in all three dimensions. The spatial confinement of a particle of mass m to a region in a given direction (say, along the x axis) of length Δx would introduce an uncertainty in its momentum $\hbar / \Delta x$ and increase its kinetic energy by an amount $E_{QC} \sim (\Delta p_x)^2 / 2m \sim \hbar^2 / 2m(\Delta x)^2$. A simple particle-in-a-box analysis, using the Schrödinger's equation and the effective mass approximation, shows that the ground state quantum confinement energy would be $E_{QC} \sim (3\hbar^2 / 8m^*)(\pi / a)^2$, where

$m^* \equiv m_e^* m_h^* /(m_e^* + m_h^*)$ is the reduced effective mass of the electron-hole pair (m_e^* and m_h^* are respectively the effective mass of the electron and hole) [11,15].

Solar cells can be fabricated from a number of semiconductor materials, most commonly silicon (Si) – crystalline, polycrystalline, and amorphous. Solar cells are also fabricated from GaAs, GaInP, Cu(InGa)Se_2, and CdTe. Solar cell materials are chosen largely on the basis of how well their absorption characteristics match the solar spectrum and their cost of fabrication. Silicon has been a common choice due to the fact that its absorption characteristics are a fairly good match to the solar spectrum, and silicon fabrication technology is well developed as a result of its pervasiveness in the semiconductor electronics industry.

Electronic grade semiconductors are very pure crystalline materials. Their crystalline nature means that their atoms are aligned in a regular periodic array. This periodicity, coupled with the atomic properties of the component elements, is what gives semiconductors their very useful electronic properties. The silicon is in group IV in periodic table, meaning that it has four valence electrons, that is, four electrons that can be shared with neighboring atoms to form covalent bonds with those neighbors. In crystalline silicon, the atoms are arranged in a diamond lattice (carbon is also a column IV element) with tetrahedral bonding – four bonds from each atom where the angle between any two bonds is 109.5°. Perhaps surprisingly, this arrangement can be represented by two interpenetrating face-centered cubic (fcc) unit cells where the second fcc unit cell is shifted one-fourth of the distance along the body diagonal of the first fcc unit cell. The lattice constant is the length of the edges of the cubic unit cell. The entire lattice can be constructed by stacking these unit cells. A similar arrangement, the zincblende lattice, occurs in many binary III–V and II–VI semiconductors such as GaAs (a III–V compound) and CdTe (a II–VI compound). For example, in GaAs, one interpenetrating fcc unit cell is composed entirely of Ga atoms and the other entirely of As atoms. Note that the average valency is four for each compound, so that there are four bonds to and from each atom with each covalent bond involving two valence electrons. Some properties of semiconductors are dependent on the orientation of the crystal lattice, and casting the crystal structure in terms of a cubic unit cell makes identifying the orientation easier using Miller indices.

Of more consequence to the physics of solar cells, however, is how the periodic crystalline structure of the semiconductor establishes its electronic properties. An electron moving in a semiconductor material is analogous to a particle confined to a three-dimensional box that has a complex interior structure due primarily to the potential fields surrounding the component atom's nucleus and tightly bound core electrons. The dynamic behavior of the electron can be established from the electron wave function, ψ, which is obtained by solving the time-independent Schrodinger equation [10-13]

$$\nabla^2\psi + \frac{2m}{\hbar^2}\left[E - U(\vec{r})\right]\psi = 0 \qquad (2.2)$$

where m is electron mass, $\hbar$ is the reduced Planck constant, E is the energy of the electron, and $U(\vec{r})$ is the periodic potential energy inside the semiconductor. Solving this quantum-mechanical equation is beyond the scope of this work, but suffice it to say that the solution defines the band structure (the allowed electron energies and the relationship between the electron's energy and momentum) of the semiconductor and, amazingly, tells us that the quantum mechanically computed motion of the electron in the crystal is, to a good approximation, like that of an electron in free space if its mass, m, is replaced by an effective mass, m∗, in Newton's law of motion from classical mechanics

$$F = m^{*}a \tag{2.3}$$

where F is the applied force and a is the acceleration of the electron. A simplified energy band structure is illustrated in Figure 2.2. The allowed electron energies are plotted against the crystal momentum, $p = \hbar k$, where k is the wave vector corresponding to the wave function solutions of the Schrodinger equation. Only the energy bands of immediate interest are shown energy bands below the valence band are presumed to be fully occupied by electrons and those above the conduction band are presumed to be empty. The electron effective mass is thus defined as

$$m^{*} \equiv \left[\frac{d^2E}{dp^2}\right]^{-1} = \left[\frac{1}{\hbar^2}\frac{d^2E}{dk^2}\right]^{-1} \tag{2.4}$$

Notice that the effective mass is not constant within each band. In addition, near the top of the valence band, the effective mass is actually negative. Electrons (∗) fill the states from bottom to top and the states near the top of the valence band are empty (o) due to some electrons being thermally excited into the conduction band. These empty states can conveniently be regarded as positively charged carriers of current called holes with a positive effective mass. It is conceptually much easier to deal with a relatively few number of holes that have a positive effective mass since they will behave like classical positively charged particles. The top of the valence band and the bottom of the conduction band are approximately parabolic in shape and therefore the electron effective mass (m_e^*) near the bottom of the conduction band is a constant, as is the hole effective mass (m_h^*) near the top of the valence band.

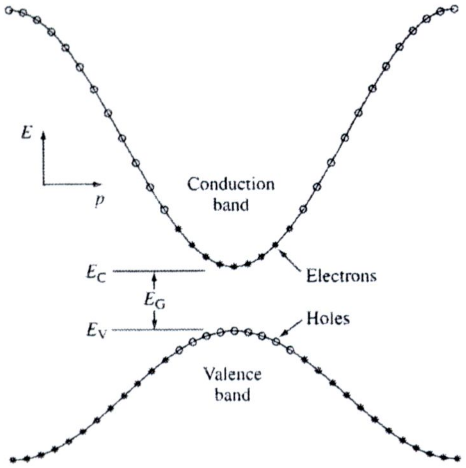

Figure 2.2 A simplified energy band diagram at T> 0 K for a direct band gap (E_g) semiconductor

This is a very practical assumption that greatly simplifies the analysis of semiconductors. When the minimum of the conduction band occurs at the same value of the crystal momentum as the maximum of the valence band, as it does in Figure 2.2, the semiconductor is a direct band gap semiconductor. When they do not align, the semiconductor is said to be an indirect band gap semiconductor.

Now that the dynamics of the electron motion in a semiconductor has been approximated by a negatively charged particle with mass m_e^* in the conduction band and by a positively charged particle with mass m_h^* in the valence band, it is possible to calculate the density of states in each band. This again involves solving the time-independent Schrodinger equation for the wave function of a particle in a box, but in this case the box is empty. All the complexities of the periodic potentials of the component atoms have been incorporated into the effective mass. The density of states in the conduction band is given by

$$g_c(E) = \frac{1}{2\pi^2}\left(\frac{2m_e^*}{\hbar^2}\right)^{\frac{3}{2}}(E - E_c)^{\frac{1}{2}} \tag{2.5}$$

while the density of states in the valence band is given by

$$g_V(E) = \frac{1}{2\pi^2}\left(\frac{2m_h^*}{\hbar^2}\right)^{\frac{3}{2}}(E_V - E)^{\frac{1}{2}} \tag{2.6}$$

2.1.2 Equilibrium carrier concentrations [14]

When the semiconductor is in thermal equilibrium (i.e. at a constant temperature with no external injection or generation of carriers), the Fermi function determines the ratio of filled states to available states at each energy and is given by [16]

$$f(E) = \left[\exp\left(\frac{E - E_F}{k_B T}\right) + 1\right]^{-1} \tag{2.7}$$

As seen in Figure 2.3,

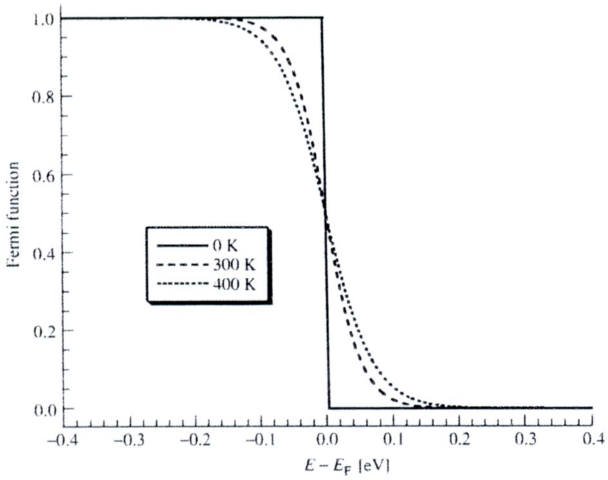

Figure 2.3 The Fermi function at various temperatures

The Fermi function is a strong function of temperature. At absolute zero, it is a step function and all the states below E_F are filled with electrons and all those above E_F are completely empty. As the temperature increases, thermal excitation will leave some states below E_F empty, and the corresponding number of states above E_F will be filled with the excited electrons.

The equilibrium electron and hole concentrations (#/cm^3) are therefore

$$n_0 = \int_{E_C}^{\infty} g_c(E) f(E) dE = \frac{2N_c}{\sqrt{\pi}} F_{1/2}\left[\frac{(E_F - E_C)}{k_B T}\right] \tag{2.8}$$

$$p_0 = \int_{-\infty}^{E_V} g_V(E)[1 - f(E)]dE = \frac{2N_V}{\sqrt{\pi}} F_{1/2}\left[\frac{(E_V - E_F)}{k_B T}\right] \tag{2.9}$$

where $F_{1/2}(\xi)$ is the Fermi–Dirac integral of order 1/2,

$$F_{1/2}(\xi) = \int_0^{\infty} \frac{\sqrt{\xi'} d\xi'}{1 + e^{\xi' - \xi}} \tag{2.10}$$

The conduction-band and valence-band effective densities of state (#/cm^3), N_C and N_V, respectively, are given by

$$N_C = 2\left(\frac{2\pi m_e^* k_B T}{h^2}\right)^{3/2} \tag{2.11}$$

$$N_V = 2\left(\frac{2\pi m_h^* k_B T}{h^2}\right)^{3/2} \tag{2.12}$$

When the Fermi energy, E_F, is sufficiently far (>3 $k_B T$) from either bandedge, the carrier concentrations can be approximated (to within 2%) as [5, 7-8]

$$n_0 = N_C e^{(E_F - E_C)/k_B T} \tag{2.13}$$

$$p_0 = N_V e^{(E_V - E_F)/k_B T} \tag{2.14}$$

and the semiconductor is said to be nondegenerate. In nondegenerate semiconductors, the product of the equilibrium electron and hole concentrations is independent of the location of the Fermi energy and is just

$$p_0 n_0 = n_i^2 = N_C N_V e^{(E_V - E_C)/k_B T} = N_C N_V e^{-E_g / k_B T} \qquad (2.15)$$

In an undoped (intrinsic) semiconductor in thermal equilibrium, the number of electrons in the conduction band and the number of holes in the valence band are equal; $n_o = p_o = n_i$, where n_i is the intrinsic carrier concentration. The intrinsic carrier concentration can be computed from (2.15), giving

$$n_i = \sqrt{N_C N_V} e^{(E_V - E_C)/2k_B T} = \sqrt{N_C N_V} e^{-E_g / 2k_B T} \qquad (2.16)$$

The Fermi energy in an intrinsic semiconductor, $E_i = E_F$, is given by

$$E_i = \frac{E_V + E_C}{2} + \frac{k_B T}{2} \ln\left(\frac{N_V}{N_C}\right) \qquad (2.17a)$$

$$E_i = \frac{E_V + E_C}{2} + \frac{3k_B T}{4} \ln\left(\frac{m_h^*}{m_e^*}\right) \qquad (2.17b)$$

Which is typically very close to the middle of the band gap. The intrinsic carrier concentration is typically very small compared to the densities of states and typical doping densities ($n_i \approx 10^{10}$ cm^{-3} in Si) and intrinsic semiconductors behave very much like insulators; that is, they are not very useful as conductors of electricity.

The number of electrons and holes in their respective bands, and hence the conductivity of the semiconductor, can be controlled through the introduction of specific impurities, or dopants, called donors and acceptors. For example, when semiconductor silicon is doped with phosphorous, it can be seen that phosphorous is in column V of the periodic table of elements and thus has five valence electrons. Four of these are used to satisfy the four covalent bonds of the silicon lattice and the fifth is available to fill an empty state in the conduction band. If silicon is doped with boron (valency of three, since it is in column III), each boron atom accepts an electron from the valence band, leaving behind a hole. All impurities introduce additional localized electronic states into the band structure, often within the forbidden band between E_C and E_V, as illustrated in Figure 2.4.

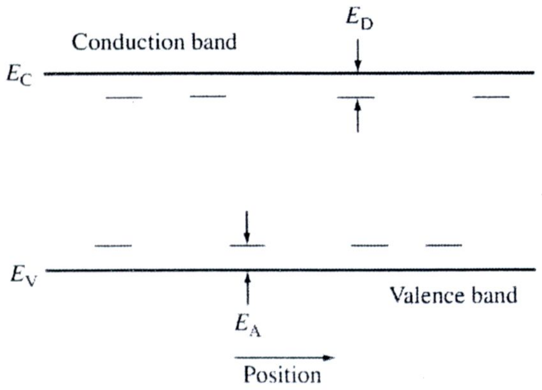

Figure 2.4 Donor and acceptor levels in a semiconductor.

If the energy of the state, E_D, introduced by a donor atom is sufficiently close to the conduction bandedge (within a few k_BT), there will be sufficient thermal energy to allow the extra electron to occupy a state in the conduction band. The donor state will then be positively charged (ionized) and must be considered when analyzing the electrostatics of the situation. Similarly, an acceptor atom will introduce a negatively charged (ionized) state at energy E_A. The controlled introduction of donor and acceptor impurities into a semiconductor allows the creation of the n-type (electrons are the primary source of electrical conduction) and p-type (holes are the primary source of electrical conduction) semiconductors, respectively. This is the basis for the construction of all semiconductor devices, including solar cells. The number of ionized donors and acceptors are given by [12, 14, 17]

$$N_D^+ = \frac{N_D}{1+g_D e^{(E_F-E_D)/k_BT}} = \frac{N_D}{1+e^{(E_F-E_D')/k_BT}} \tag{2.18}$$

$$N_A^- = \frac{N_A}{1+g_A e^{(E_A-E_F)/k_BT}} = \frac{N_A}{1+e^{(E_A'-E_F)/k_BT}} \tag{2.19}$$

where g_D and g_A are the donor and acceptor site degeneracy factors. Typically, $g_D = 2$ and $g_A = 4$. These factors are normally combined into the donor and the acceptor energies so that $E_D' = E_D - k_BT \ln g_D$ and $E_A' = E_A - k_BT \ln g_A$ Often, the donors and acceptors are assumed to be completely ionized so that $n_0 \approx N_D$ in n-type material and $p_0 \approx N_A$ in p-type material. The Fermi energy can then be written as

$$E_F = E_i + \frac{k_BT}{2} \ln\left(\frac{N_D}{n_i}\right) \tag{2.20}$$

in n-type material and as

$$E_F = E_i - \frac{k_BT}{2} \ln\left(\frac{N_A}{n_i}\right) \tag{2.21}$$

THE NATIONAL RESEARCH COUNCIL OF THAILAND
RESEARCH LIBRARY

in p-type material.

When a very large concentration of dopants is introduced into the semiconductor, the dopants can no longer be thought of as a minor perturbation to the system. Their effect on the band structure must be considered.

2.1.3 Light absorption

The creation of electron–hole pairs via the absorption of sunlight is fundamental to the operation of solar cells. The excitation of an electron directly from the valence band (which leaves a hole behind) to the conduction band is called fundamental absorption. Both the total energy and momentum of all particles involved in the absorption process must be conserved. Since the photon momentum, $p_\lambda = h/\lambda$, is very small compared to the range of the crystal momentum (The wavelength of sunlight, λ, is on the order of a micron (10^{-4} cm), while the lattice constant is a few angstroms (10^{-8} cm). Thus, the crystal momentum is several orders of magnitude larger than the photon momentum.), the photon absorption process must, for practical purposes, conserve the momentum of the electron.

The absorption coefficient for a given photon energy, hv, is proportional to the probability, P_{12}, of the transition of an electron from the initial state E_1 to the final state E_2, the density of electrons in the initial state, $g_C(E_2)$, and the density of available final states, $g_V(E_1)$.

$$\alpha(h\nu) \propto \sum P_{12} g_V(E_1) g_C(E_2) \qquad (2.22)$$

assuming that all the valence-band states are full and all the conduction-band states are empty. Absorption results in creation of an electron-hole pair since a free electron is excited to the conduction band leaving a free hole in the valence band.

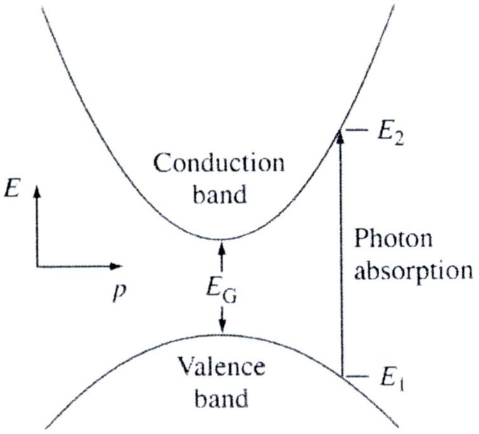

Figure 2.5 Photon absorption in a direct band gap semiconductor for an incident photon with energy hv > E_g

In direct band gap semiconductors, such as GaAs, GaInP, CdTe, and Cu(InGa)Se$_2$, the basic photon absorption process is illustrated in Figure 2.5. Both energy and momentum must be conserved in the transition.

Every initial electron state with energy E$_1$ and crystal momentum p$_1$ in the valence band is associated with a final state in the conduction band at energy E$_2$ and crystal momentum p$_2$. Since the electron momentum is conserved, the crystal momentum of the final state is the same as the initial state, $p_1 \approx p_2 = p$. Conservation of energy dictates that the energy of the absorbed photon is

$$h\nu = E_2 - E_1 \tag{2.23}$$

Since we have assumed parabolic bands,

$$E_V - E_1 = \frac{p^2}{2m_h^*} \tag{2.24}$$

$$E_2 - E_C = \frac{p^2}{2m_e^*} \tag{2.25}$$

Combining equations (2.23), (2.24), and (2.25) yields

$$h\nu - E_g = \frac{p^2}{2}\left(\frac{1}{m_e^*} + \frac{1}{m_h^*}\right) \tag{2.26}$$

and the absorption coefficient for direct transitions is [1, 22-24]

$$\alpha(h\nu) \approx A^*\left(h\nu - E_g\right)^{1/2} \tag{2.27}$$

where A* is a constant. In some semiconductor materials, quantum selection rules do not allow transitions at p = 0 but allow them for $p \neq 0$. In such cases [12]

$$\alpha(h\nu) \approx \frac{B^*}{h\nu}\left(h\nu - E_g\right)^{3/2} \tag{2.28}$$

where B* is a constant.

In indirect band gap semiconductors like Si and Ge, where the valence-band maximum occurs at a different crystal momentum than the conduction-band minimum, conservation of electron momentum necessitates that the photon absorption process involve an additional particle. Phonons, the particle representation of lattice vibrations in the semiconductor, are suited to this process because they are low-energy particles with relatively high momentum. This is illustrated in Figure 2.6.

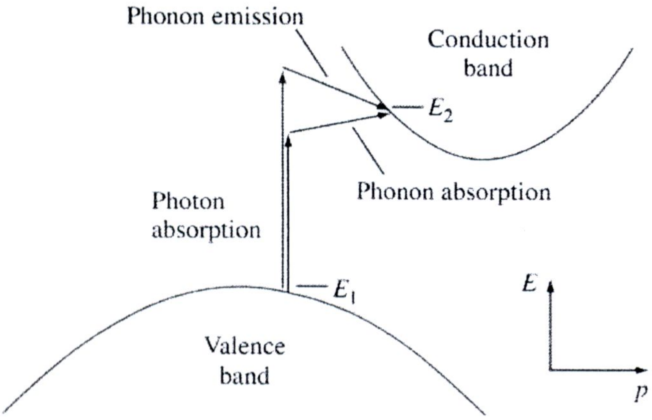

Figure 2.6 Photon absorption in an indirect band gap semiconductor for a photon with energy hν $<$ $E_2 - E_1$ and a photon with energy hν $>$ $E_2 - E_1$. Energy and momentum in each case are conserved by the absorption and emission of a phonon, respectively

Notice that light absorption is facilitated by either phonon absorption or phonon emission. The absorption coefficient, when there is phonon absorption, is given by

$$\alpha_a(h\nu) = \frac{A(h\nu - E_g + E_{ph})^2}{e^{E_{ph}/k_BT} - 1} \tag{2.29}$$

$$\alpha_e(h\nu) = \frac{A(h\nu - E_g - E_{ph})^2}{1 - e^{-E_{ph}/k_B T}} \tag{2.30}$$

when a phonon is emitted [10]. Because both processes are possible,

$$\alpha(h\nu) = \alpha_a(h\nu) + \alpha_e(h\nu) \tag{2.31}$$

In both direct band gap and indirect band gap materials, a number of photon absorption processes are involved, though the mechanisms described above are the dominantones. A direct transition, without phonon assistance, is possible in indirect band gap materials if the photon energy is high enough. Conversely, in direct band gap materials, phonon-assisted absorption is also a possibility. Other mechanisms may also play a role in defining the absorption process in semiconductors.

2.1.4 Luminescence and light emission in solids [1, 19]

Atoms emit light or photons by spontaneous emission when electrons in excited states transition to a lower level. In solids the radiative emission process is called luminescence. Luminescence can occur by a number of mechanisms such as photoluminescence, that the re-emission of light after absorbing a photon of higher energy and electroluminescence, that the emission of light caused by continuous an electrical current through the material. The physical processes involved in both photoluminescence and electroluminescence are more involved than the certain in absorption. This is because the generation of light by luminescence is affectionately tied up with the energy relaxation mechanisms in the solid. In addition, the shape of the emission spectrum is influenced by thermal distribution of the electrons and holes within their bands. Hence, we have to consider the emission rates and thermal extended of the carriers before we can gain a good understanding of the emission efficiency and the luminescence spectrum. The main processes occur when light is emitted from a solid shown that in Figure 2.7.

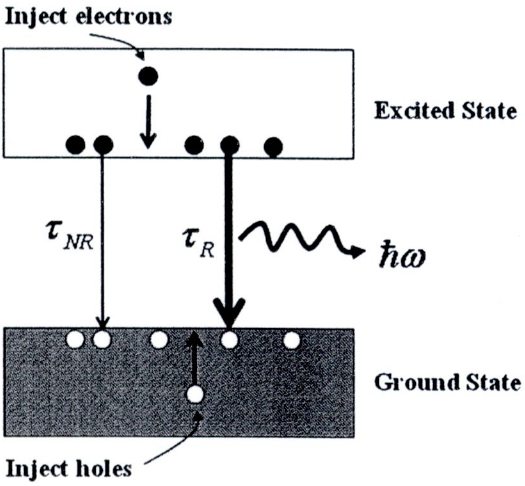

Figure 2.7 General scheme of luminescence in a solid

The photon is emitted when an electron in excited state drops down into an empty state in the ground state band. For this to be possible, we must first inject electrons, which then relax to the state from where the emission occurs. This could be the bottom of the conduction band, but it might also be a discrete level. The photon cannot be emitted except the lower level for the transition is empty, because the Pauli principle does not permit us to put two electrons into the same level. The empty lower level is produced by injecting holes into the ground state band in an entirely analogous way to the injection of electrons into the excited state.

We can summarize these points by writing the luminescence intensity at frequency ν as

$$I(h\nu) \propto |M|^2 g(h\nu) \times (LOF) \qquad (2.32)$$

where *LOF* is level occupancy factors, give the probabilities that the significant upper level is occupied and lower level is empty. The other two terms are the matrix element and density of states for the transition, which determine the quantum mechanical transition probability by Fermi's golden rule [13,17]. The electrons relax very rapidly to the lowest levels within the excited state band, and the form a thermal distribution that can be calculated by statistical mechanics. In normal circumstances the electrons will relax to within ~ k_BT of the bottom of the excited state band. The light is emitted between the electron and hole states that are thermally occupied, and will therefore only be emitted within a narrow energy range from the lowest levels in the excited state band. This contrasts with the absorption spectrum, where photons can be absorbed to any state within the excited state band.

Radiative emission is not the only mechanism by which the electrons in an excited state can drop down to the ground state. The alternative pathway between the excited state and ground state band in Figure 2.7 indicates the possibility of non-radiative relaxation. The electron might, for example, lose its excitation energy as heat by emitting phonons, or it may transfer the energy to impurities or defects called "traps". If these non-radiative relaxation processes occur on a faster time scale than the radiative transitions, very little light will be emitted.

2.1.5 Interband luminescence of direct gap materials [18]

Interband luminescence occur in a semiconductor when an electron that has been excited into the conduction band drop back to the valence band by the emission of a photon. This at the same time reduces the number of electrons in the conduction band and holes in the valence band by one. Interband luminescence thus corresponds to the annihilation of an electron-hole pair, and is known as radiative electron-hole recombination. This should be contrasted with interband absorption, which is equivalent to the creation of an electron-hole pair. Figure 2.8 shows the band diagram for an interband luminescence process in a direct gap semiconductor.

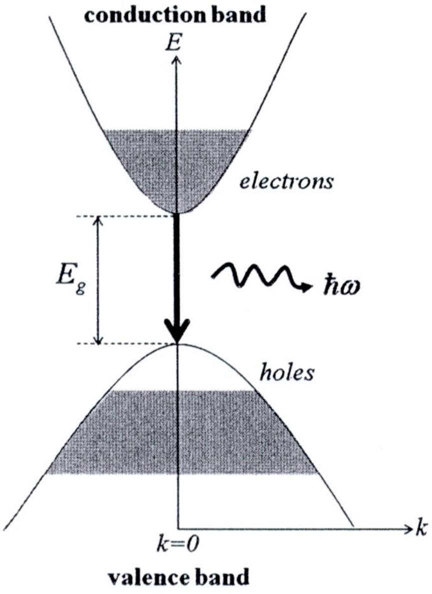

Figure 2.8 the interband luminescence process in a direct gap semiconductor

The photons are emitted when electrons at the bottom of the conduction band recombine with holes at the top of the valence band. The optical transitions between the valence and conduction bands of typical direct gap semiconductors are dipole allowed and large matrix elements. The radiative lifetime will be short, with typical values in the range $10^{-8} - 10^{-9}$ s. The luminescence efficiency is therefore expected to be high. The processes which the electrons and holes are injected into the bands relax very rapidly to the lowest energy states within their respective bands by emitting photons. This means that the electrons accumulate at the bottom of the conduction band before they recombine, the holes accumulate at the top of the valence band.

Since the momentum of the photon is negligible compared to the momentum of the electron, the electron and hole that recombine must have the same k vector. Therefore, the transition is represented by a downward vertical arrow on the band diagram as show in figure 2.8. The emission takes place near k=0, and corresponds to a photon of energy E_g. No matter how we excite the electrons and holes in the first place, we always obtain luminescence at energies close to the band gap. The luminescence spectrum consists of a narrow emission line close to the band gap energy, while the absorption shows the usual threshold at E_g with continuous absorption for $h\nu > E_g$.

2.1.6 Photoluminescence of direct gap materials [1,2]

The re-emission of light by interband luminescence after a direct gap semiconductor has been excited by a photon with energy greater than E_g, this process is called photoluminescence.

The band diagram show that in Figure 2.9 corresponding to the photoluminescence process in a direct gap material, which photons are absorbed from an excitation source is chosen so that $h\nu_L$ is greater than E_g. The electrons are initially created in states high up in the conduction band. The electrons do not remain in these initial states for very long, because they can lose their energy very rapidly by emitting phonons. This process is indicated by the cascade of transitions within the conduction band. Each step corresponds to the emission of phonon with the correct energy and momentum to satisfy the conservation laws.

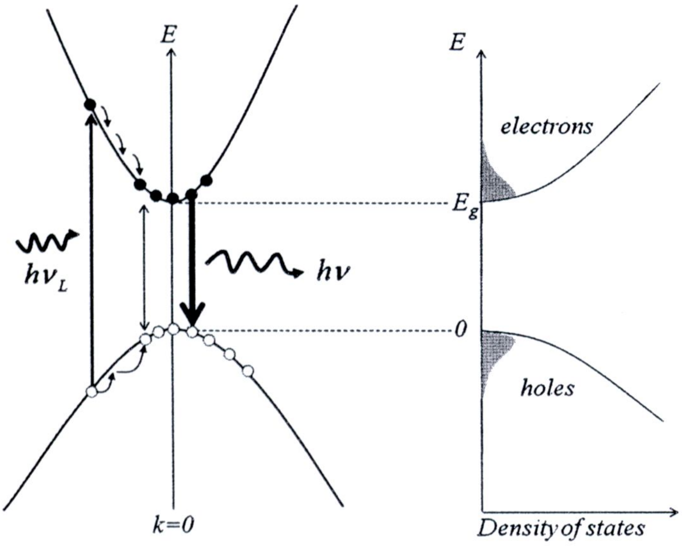

Figure 2.9 the processes occurring during photoluminescence in a direct gap semiconductor after excitation at frequency ν_L

The electron-phonon coupling in most solids is very strong and these scattering events take place on time scales as short as ~100 fs. This is much faster than the radiative lifetimes which are in the nanosecond range, and the electrons are therefore able to relax to the bottom of the conduction band long before they have had time to emit photons. The same conditions apply to the relaxation of the holes in the valence band.

After the electrons and holes have relaxed as far as they can by phonon emission, they must wait at the bottom of the bands until they can emit a photon or recombine non-radiatively. This leaves time to thermal distributions, as sketched in Figure 2.9. The shading indicates the occupancy of the available states. These occupancy factors can be calculated by applying statistical physics to the electron and hole distributions.

The distributions of the optically excited electrons and holes in their bands can be calculated by Fermi-Dirac statistics. The total number density N_e of electrons is determined by the power of the illumination source and must satisfy the following equation

$$N_e = \int_{E_g}^{\infty} g_c(E) f_e(E) dE \tag{2.33}$$

where $g_c(E)$ is the density of states in the conduction band.

$$g_c(E) = \frac{1}{2\pi^2}\left(\frac{2m_e^*}{\hbar^2}\right)^{\frac{3}{2}} \left(E - E_g\right)^{\frac{1}{2}} \tag{2.34}$$

$f_e(E)$ is the Fermi-Dirac distribution for the electrons.

$$f_e(E) = \left[\exp\left(\frac{E - E_F^c}{k_B T}\right) + 1\right]^{-1} \tag{2.35}$$

A subscript c to the Fermi level E_F to indicate that it only applies to the electrons in the conduction band. This is needed because we are in a situation of quasi-equilibrium in which there is no unique Fermi energy, and the electrons and holes have different Fermi levels.

The Fermi integral can be put in a more transparent form by changing the variables such that we start the electron energy at the bottom of the conduction band. Then combine equations 2.33-2.35 to obtain.

$$N_e = \int_0^{\infty} \frac{1}{2\pi^2}\left(\frac{2m_e^*}{\hbar^2}\right)^{\frac{3}{2}} E^{\frac{1}{2}} \left[\exp\left(\frac{E - E_F^c}{k_B T}\right) + 1\right]^{-1} dE \tag{2.36}$$

Where E_F^c is now measured relative to the bottom of the conduction band. In the same way, we can write for the holes,

$$N_h = \int_0^\infty \frac{1}{2\pi^2}\left(\frac{2m_h^*}{\hbar^2}\right)^{\frac{3}{2}} E^{\frac{1}{2}}\left[\exp\left(\frac{E-E_F^V}{k_BT}\right)+1\right]^{-1} dE \qquad (2.37)$$

where $E=0$ corresponds to the top of the valence band and the energy is measured downwards. The Fermi energy for the holes E_F^V is also measured downwards from the top of the valence band. Note that N_e must equal N_h here because the photoexcitation process creates equal numbers of electrons and holes. The Fermi energies can be calculated explicitly and are given by

$$E_F^{c,V} = \frac{\hbar^2}{2m_{e,h}^*}\left(3\pi^2 N_{e,h}\right)^{\frac{2}{3}} \qquad (2.38)$$

2.1.7 Photoluminescence for low carrier densities

At low carrier densities (high temperature), the electron and hole distributions will be described by classical statistics. The occupancies are then just given by Boltzmann statistics

$$f(E) \propto \exp\left(-\frac{E}{k_BT}\right) \qquad (2.39)$$

The frequency dependence of the emission spectrum in the classical limit can be calculated if we assume that the matrix element in (2.32) is independent of frequency. We can evaluate all the factors in (2.32) and obtain.

$$I(h\nu) \propto \left(h\nu - E_g\right)^{1/2} \exp\left(-\frac{h\nu - E_g}{k_BT}\right) \qquad (2.40)$$

The $\left(h\nu - E_g\right)^{1/2}$ factor arises from the density of states for the interband transition. The final factor arises from the Boltzmann statistics of the electrons and holes. The luminescence spectrum described by (2.40) rise sharply at E_g and then fall off exponentially with a decay constant of $k_B T$ due to Boltzmann statistics factor. We thus expect a sharply peaked spectrum of width ~ $k_B T$ starting at E_g.

2.2 Physics of the solar cell [12-14]

Semiconductor solar cells are fundamentally quite simple devices. Semiconductors have the capacity to absorb light and to deliver a portion of the energy of the absorbed photons to carriers of electrical current – electrons and holes. A semiconductor diode separates and collects the carriers and conducts the generated electrical current preferentially in a specific direction. Thus, a solar cell is simply a semiconductor diode that has been carefully designed and constructed to efficiently absorb and convert light energy from the sun into electrical energy. A simple conventional solar cell structure is depicted in Figure 2.10. Sunlight is incident from the top on the front of the solar cell. A metallic grid forms one of the electrical contacts of the diode and allows light to fall on the semiconductor between the grid lines and thus be absorbed and converted into electrical energy. An antireflective layer between the grid lines increases the amount of light transmitted to the semiconductor. The semiconductor diode is fashioned when an n-type semiconductor and a p-type semiconductor are brought together to form a metallurgical junction. This is typically achieved through diffusion or implantation of specific impurities (dopants) or via a deposition process. The diode's other electrical contact is formed by a metallic layer on the back of the solar cell.

All electromagnetic radiation, including sunlight, is composed of particles called photons, which carry specific amounts of energy determined by the spectral properties of their source. Photons also exhibit a wavelike character with the wavelength, λ, being related to the photon energy related to the photon energy, E_λ, by

$$E_\lambda = \frac{hc}{\lambda} \tag{2.41}$$

where h is Plank's constant and c is the speed of light. Only photons with sufficient energy to create an electron–hole pair, that is, those with energy greater than the semiconductor band gap (E_g), will contribute to the energy conversion process. Thus, the spectral nature of sunlight is an important consideration in the design of efficient solar cells.

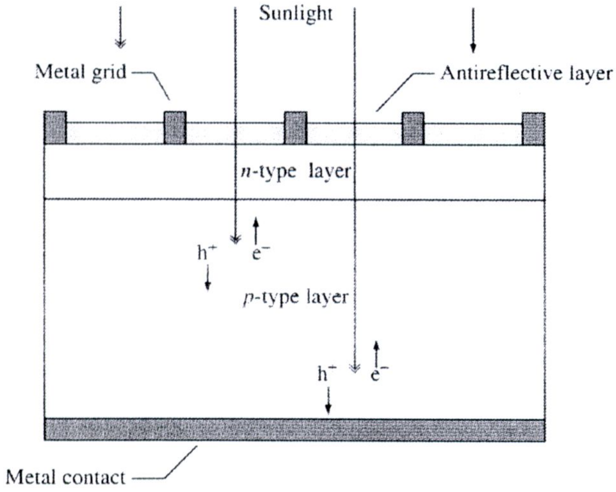

Figure 2.10 A schematic of a simple conventional solar cell. Creation of electron–hole pairs, e– and h+, respectively, is depicted

The sun has a surface temperature of 5762 K and its radiation spectrum can be approximated by a black-body radiator at that temperature. Emission of radiation from the sun, as with all black-body radiators, is isotropic. However, the Earth's great distance from the sun (approximately 93 million miles) means that only those photons emitted directly in the direction of the Earth contribute to the solar spectrum as observed from Earth. Therefore, for practical purposes, the light falling on the Earth can be thought of as parallel streams of photons. Just above the Earth's atmosphere, the radiation intensity, or Solar Constant, is about 1.353 kW/m^2 [16] and the spectral distribution is referred to as an air mass zero (AM0) radiation spectrum. The Air Mass is a measure of how absorption in the atmosphere affects the spectral content and intensity of the solar radiation reaching the Earth's surface. The Air Mass number is given by

$$AM = \frac{1}{\cos\theta} \tag{2.42}$$

where θ is the angle of incidence ($\theta = 0$ when the sun is directly overhead). The Air Mass number is always greater than or equal to one at the Earth's surface. An easy way to estimate the Air Mass has been given by Green [46-49] as

$$AM = \sqrt{1 + (S/H)^2} \tag{2.43}$$

where S is the length of a shadow cast by an object of height H. A widely used standard for comparing solar cell performance is the AM1.5 spectrum normalized to a total power density of 1 kW/m^2. The spectral content of sunlight at the Earth's surface also has a diffuse (indirect) component owing to scattering and reflection in the atmosphere and surrounding landscape and can account for up to 20% of the light incident on a solar cell. The Air Mass number is therefore further defined by whether or not the measured spectrum includes the diffuse component. An AM1.5g (global) spectrum includes the diffuse component, while an AM1.5d (direct) does not. Black body ($T = 5762$ K), AM0, and AM1.5g radiation spectrums are shown in Figure 2.11.

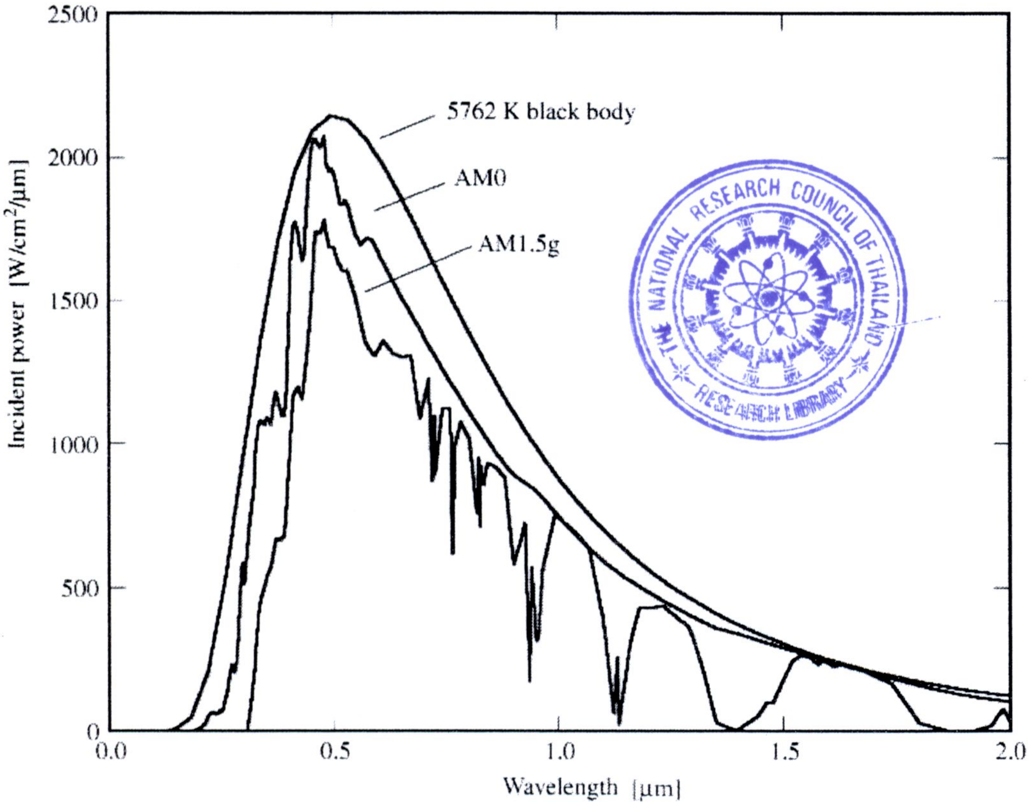

THE NATIONAL RESEARCH COUNCIL OF THAILAND
RESEARCH LIBRARY

Figure 2.11 The radiation spectrum for a black body at 5762 K, an AM0 spectrum, and an AM1.5 global spectrum

2.2.1 Basic Structures for photovoltaic action

The key material in a solar cell is the absorber. These materials are capable of absorption-caused excited states produced by photons with energies in the photon-rich range of the solar spectrum. The resulting excited states must be mobile; i.e., free electron-hole pairs, which can be separated, or excitons, which can be disassociated into free electrons and free holes and separated. Absorber materials can be organic or inorganic semiconductors, dye molecules, or quantum dots, which are the man-made inorganic particle equivalent of dye molecules. In some configurations, the absorption and separation are both accomplished in the same material. In these cases there is a region in the absorber with a built-in electric field designed to break symmetry thereby forcing electrons in one direction and holes in the other. We will term this region a junction. In other configurations a second material is used with the absorber to set up the symmetry-breaking region. In this case the symmetry-breaking may be accomplished with an electric field, effective fields, or both. We will also refer to such regions as junctions.

Before we actually start assembling the band diagrams of the structures we will use to explore the electric field, effective field, and diffusion sources of photovoltaic action, we should first review the rules for constructing band diagrams for multi-component material systems in thermodynamic equilibrium (TE). To do that, we make use of Figure 2.12, which shows two semiconductors in various stages of forming a materials system in TE. The materials are isolated from one another and their band diagrams are lined up in Figure 2.12a with respect to the vacuum (escape) level so that we can see the relative positions of the bands and energy gaps. Figure 2.12a also shows the positions of the Fermi levels in each material—again with respect to the common reference of the vacuum level–using the workfunctions ϕ_{W1} and ϕ_{W2}. As can be seen in Figure 2.12a, material 1 is n-type and material 2 is p-type. The quantities V_n and V_p also locate the Fermi levels but they do not use a common reference; i.e., V_n locates the Fermi level of material 1 with respect to the conduction band edge of material 1 while V_p locates the Fermi level of material 2 with respect to the valence band edge of material 2.

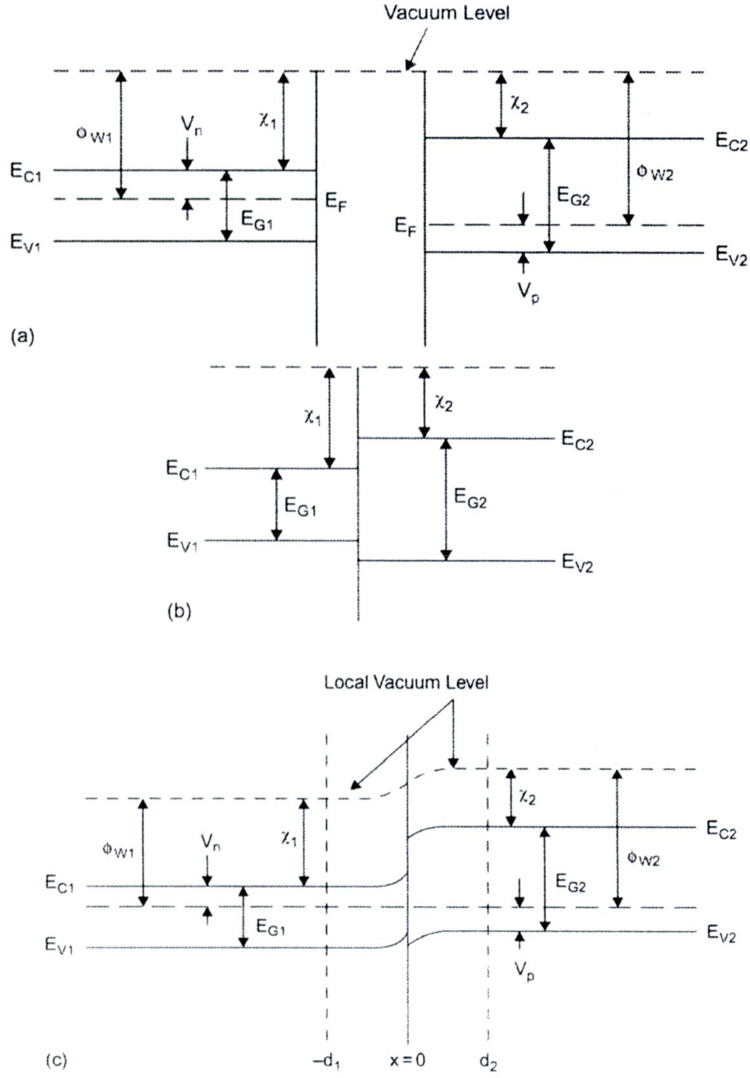

Figure 2.12 (a) Two semiconductors prior to contact, (b) the same two semiconductors during contact and (c) the same two semiconductors after contact, in thermodynamic equilibrium.

Figure 2.12b is part of a thought experiment in which we place these two materials together (actually one would be deposited or grown on the other) and watch them begin to come into thermodynamic equilibrium. Of course, TE is that very special situation for which a system of materials has one temperature and one Fermi level. Since they have not come into TE in Figure 2.12b, we do not draw the Fermi levels but, thanks to Figure 2.12a, we can certainly see how the band edges and vacuum level line up on contact. Since we are forming an abrupt interface in this example, there are abrupt steps in the electron affinity χ and hole affinity $E_g + \chi$ at the x = 0 position. These steps would be graded if one material were graded into the other. Figure 2.12c shows the continuation of the thought experiment where we have allowed the materials system to come to TE, with one Fermi level and one temperature. As seen, far to the left of the junction region, the Fermi level has its old position with respect to the local vacuum level, as shown by ϕ_{W1}, and its old position in the band gap of material 1, as and shown by V_n. Far to the right of the junction, the Fermi level also has its old position with respect to the local vacuum level, as shown by ϕ_{W2}, and its old position in the band gap of material 2, as shown by V_p. This must be the case, since V_n and V_p are dictated by doping far from a metallurgical junction and the affinities cannot change for a given material. Establishing one Fermi level for the system in TE is accomplished by the creation of an electrostatic potential energy between x = -d1 and x = d2 or, correspondingly, by the creation of a new potential energy component for electrons. Remembering that band diagrams show total energy levels for electrons, we see that this electron potential energy shifts the energy levels of material 2 up with respect to those of material 1 (or shifts the energy levels of material 1 down with respect to those ofmaterial 2) just enough to equate the Fermi level across the whole materials system. The electron potential energy being developed between x = −d1 and x = d2 is seen in the band bending in this region; i.e., the valence bands, conduction bands, and local vacuum level are all bending due to the presence of this newly created electron potential energy. The orientation of the electron potential energy difference across the junction, which is typically called the built-in potential, tells us that the materials system must have developed a negative charge on the right side of the interface and thus a positive charge on the left side of the interface. This can be seen by the conduction band's bending toward, and the valence band's bending away from, the Fermi level in material 2 (resulting in a net negative charge), and by the conduction band's bending away from, and the valence band's bending toward, the Fermi level in material 1 (resulting in a net positive charge). The local vacuum level $E_{VL}(x)$ with position is the built-in electrostatic field creating the built-in electron potential energy. The total variation in E_{VL} across the dipole (i.e., the band bending from $x = -d1$ to $x = d2$ in Fig. 2.12c) is the built-in potential V_{bi}. It is the sum of V_{bi1}, the band bending in material 1, plus V_{bi2}, the band bending in material 2; i.e.,

$$V_{bi} = V_{bi1} + V_{bi2} \tag{2.44}$$

As shown in Figure 2.12a, the work function difference is what forces the creation of V_{bi}. Consequently,

$$V_{bi} = \phi_{w2} - \phi_{w1} \tag{2.45}$$

2.2.2 PN-junction [12-14]

Where an n-type semiconductor comes into contact with a p-type semiconductor, a pn-junction is formed. In thermal equilibrium there is no net current flow and by definition the Fermi energy must be independent of position. Since there is a concentration difference of holes and electrons between the two types of semiconductors, holes diffuse from the p-type region into the n-type region and, similarly, electrons from the n-type material diffuse into the p-type region. As the carriers diffuse, the charged impurities (ionized acceptors in the p-type material and ionized donors in the n-type material) are uncovered – that is, no longer screened by the majority carrier. As these impurity charges are uncovered, an electric field (or electrostatic potential difference) is produced, which limits the diffusion of the holes and electrons. In thermal equilibrium, the diffusion and drift currents for each carrier type exactly balance, so there is no net current flow. The transition region between the n-type and the p-type semiconductors is called the space-charge region.It is also often called the depletion region, since it is effectively depleted of both holes and electrons. Assuming that the p-type and the n-type regions are sufficiently thick, the regions on either side of the depletion region are essentially charge-neutral (often termed quasi-neutral). The electrostatic potential difference resulting from the junction formation is called the built-in voltage, V_{bi} . It arises from the electric field created by the exposure of the positive and the negative space charge in the depletion region. The electrostatics of this situation (assuming a single acceptor and a single donor level) are governed by Poisson's equation

$$\nabla^2\phi = \frac{q}{\varepsilon}\left(n_0 - p_0 + N_A^- - N_D^+\right) \qquad (2.46)$$

where ϕ is the electrostatic potential, q is magnitude of the electron charge, ε is the electric permittivity of the semiconductor, p_o is the equilibrium hole concentration, n_o is the equilibrium electron concentration, N_A^- is the ionized acceptor concentration, and N_D^+ is the ionized donor concentration.

The depletion region extends furthest into the more lightly doped side and depletion width, W_D, gives

$$W_D = \sqrt{\frac{2\varepsilon}{q}\left(\frac{N_A + N_D}{N_A N_D}\right)V_{bi}} \qquad (2.47)$$

Under nonequilibrium conditions, the electrostatic potential difference across the junction is modified by the applied voltage, V, which is zero in thermal equilibrium. As a consequence, the depletion width is dependent on the applied voltage,

$$W_D = \sqrt{\frac{2\varepsilon}{q}\left(\frac{N_A + N_D}{N_A N_D}\right)(V_{bi} - V)} \tag{2.48}$$

As previously stated, the built-in voltage, V_{bi}, can be calculated by noting that under thermal equilibrium the net hole and electron currents are zero.

The equilibrium energy band diagram is shown that in Figure 2.13, electric field, and charge density for a simple abrupt pn-junction silicon diode in the vicinity of the depletion region. The conduction band edge is given by $E_C(x) = E_0 - q\phi(x) - \chi$, the valence band edge by $E_V(x) = E_C(x) - E_g$,

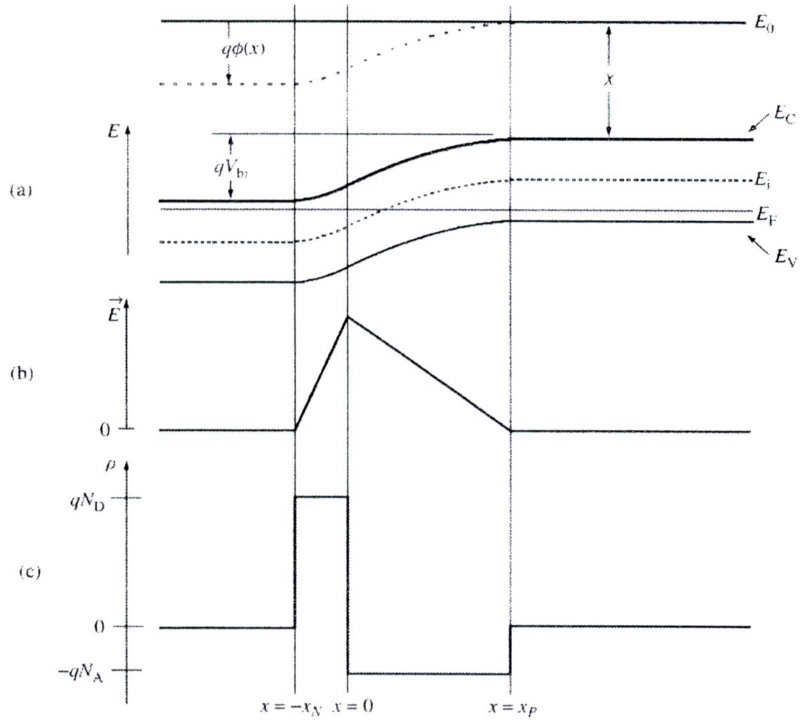

Figure 2.13 Equilibrium conditions in a solar cell: (a) energy bands; (b) electric field; and (c) charge density

2.3 Dye-sensitized solar cells (DSSCs) [12,14]

The basic function of a solar cell is to absorb incoming light, create electron-hole pairs, and transfer the charges to the collection electrodes. The concept of dye-sensitization was invented in order to find a photoelectrochemical cell based on a semiconductor, which is stable against photocorrosion and yet absorbs light in the visible region. Many semiconductor oxides like TiO_2, SnO_2 and ZnO satisfy the first requirement; however, they only absorb UV light because of their wide band gap. An alternative approach to extend their spectral response is to attach dye molecules absorbing the visible light onto the semiconductor surface: dye-sensitization. Gräzel and co-workers first achieved a breakthrough with the use of nanostructured TiO_2 films deposited on a conducting substrate.

A novel solar cell based on a dye sensitized porous nanocrystalline TiO_2 photoanode with attractive performance has been reported by Grätzel et al. [21,105]. Interest in porous semiconductor matrices permeated by an electrolyte solution containing dye and redox couples has been stimulated by their reports. The conversion efficiency of the dye sensitized solar cells (DSSCs) has been currently improved to above 11% since the first DSSCs was reported with efficiency of 7.1% [17]. Even though silicon champion cells have attained 24%, the maximum conversion efficiency is approximately 30% for both devices [81]. Large-size DSSCs has been prepared on silver grid embedded fluorine-doped tin oxide (FTO) glass substrate by screen printing method..

0 Under the standard test condition, energy conversion efficiency of active area was achieved to 5.52% in 5 cm×5 cm device, which is comparable to 6.16% of small-size cell prepared at similar condition.

In DSSCs, the initial photoexcitation does not occur in the semiconductor working electrode as the electrochemical photovoltaic cells in Scheme 1a, but occurs in the light absorbing dye as shown in Scheme 2. Subsequent injection of an electron from the photo-excited dye into the conduction band of semiconductors results in the flow of current in the external circuit. Sustained conversion of light energy is facilitated by regeneration of the reduced dye (D in Figure 2.14) either via a reversible redox couple (O/R), which is usually I_3^- / I^- (Figure 2.14a) or via the electron donation from a p-type semiconductor (Figure 2.14b) .

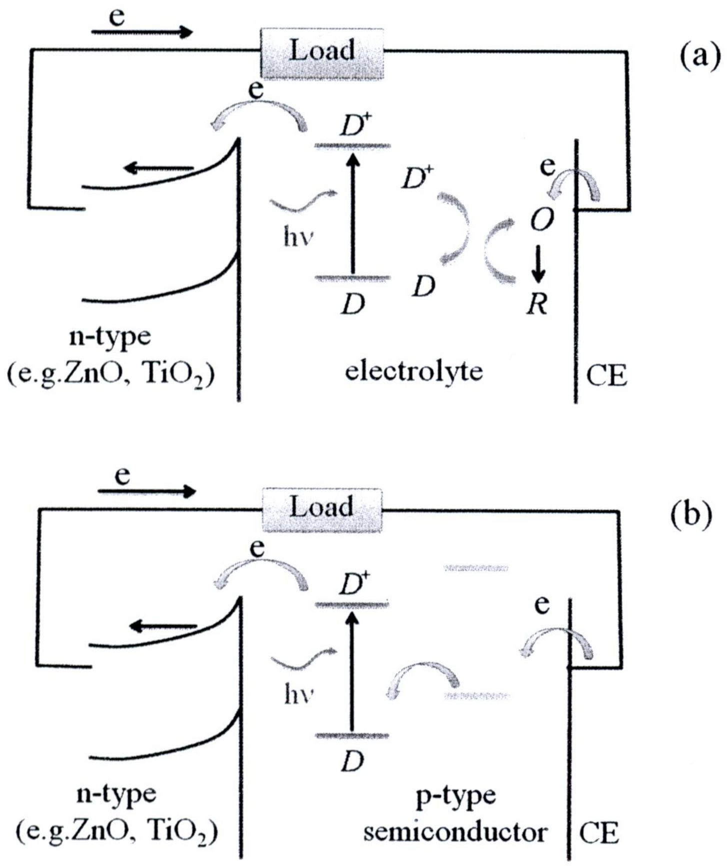

Figure 2.14 Operation mechanism of the dye sensitized electrochemical solar cell (DSSCs). D: Dye, O: Oxidant (e,g, I_3^-), R: Reductant (e.g. I^-). (a) Wet-type DSSC with redox couple in the liquid electrolyte (b) Solid state DSSCs with a p-type semiconductor to replace the electrolyte containing the redox couple.

2.3.1 Materials and structure of DSSCs

The DSSCs is composed of two electrodes, the photoelectrode and the counterelectrode. The photoelectrode consists of a dye-sensitizer adsorbed on the mesoporous semiconductor which attached to a transparent conducting substrate (TCO). The TCO is usually fluorine doped tin oxide (F: SnO_2 or FTO). The counterelectrode also consist a platinum (Pt) layer covered on FTO substrate. The gap between the electrodes is filled with a redox electrolyte, usually the mixture of iodine and iodide in organic solvent. The dye material, whether organic molecules or inorganic quantum dots, absorbs light by exciton production, the dye LUMO level must be sufficiently above the semiconductor conduction-band edge.

2.3.2 The mechanism of the DSSCs

The role of the semiconductor is mainly to provide a large surface area and transport electrons towards the collecting electrode. Key factors in device design are the careful control of morphology of the nanostructured semiconductor, leading to the efficient dissociation of generated electron-hole pairs, and subsequent transport of charge carriers. A variety of nanostructured materials, including TiO_2, SnO_2, ZnO, have been used as the oxide layer. The nanostructured semiconductor oxide exhibits a large surface area. The oxide layer provides a larger surface area for dye anchoring, and increases the interface because of the absence of a significant electrical potential gradient in the film. [85-86] In the case of TiO_2 nanoparticle film, a driving force for the electron flow, through the porous between the dye-sensitized semiconductor and the electrolyte. The charge transport properties in the DSSCs remains to be elucidated and the details around the transport mechanism are not fully understood. The macroscopic carrier transport in the nanostructured semiconductor is commonly assumed to be dominated by diffusion because of the absence of a significant electrical potential gradient in the film. [87] In the case of TiO_2 nanoparticle film, a driving force for the electron flow, through the porous network toward the conducting substrate, may be the equilibrium of the electron density through the film. Several groups have reported the existence of the sub-band gap states lying below the conduction band edge of the nanostructured TiO_2. These sub-band gap states are believed to be involved in the diffusion process and are discussed mostly in terms of a trapping/detrapping mode, and by a hopping model. The diffusion coefficient and the back reaction rate of electrons have been found to depend strongly on the electron occupation of band gap/conduction band driven states of the TiO_2 nanoparticle films. [88]

ZnO has the similar band gap and electron affinity as TiO_2, making it a possible candidate as a semiconductor oxide for DSSCs. ZnO is a direct wide-band gap semiconductor ($3d^{10}4s^2$) with a band gap of ~ 3.30 eV at room temperature.

DSSCs differ from conventional devices in that they separate the function of light absorption from charge carrier transport. The photoexcitation occurs in the dye molecules and the charge separation occurs at the dye/ZnO interface. As the different components of the DSSCs are brought into contact, they will equilibrate by exchanging charges. At dark, the Fermi levels of the working electrode and the counter electrode are in equilibrium with that of the electrolyte redox couple. When the working electrode is illuminated under open-circuit conditions, the Fermi level of the counter electrode and electrolyte is unchanged, whereas the Fermi level of the working electrode changes, producing the open-circuit voltage (V_{OC}). The energy level diagram of the cell components and electron transfer under illumination is illustrated in Figure 2.15.

When the dye sensitizer absorbs a photon and transform to excited state, an electron of dye injects to the conduction band of semiconductor or it can directly recombine back to the ground state. After a successful injection, the injected electrons diffuse through FTO and flow through the load via the external circuit and then reach the Pt counterelectrode. At the Pt counterelectrode, the oxidized redox species, I_3^-, is subsequently reduced back to I^- by accepting electron. The oxidized dye is quickly reduced back to its original state by reduce redox species (I^-) in the electrolyte for a complete cycle of electron transfer. A concentration gradient between the photoelectrode and counterelectrode of I_3^- and I^- are transport between two electrodes. The DSSCs mechanism is illustrated in Figure 2.15.

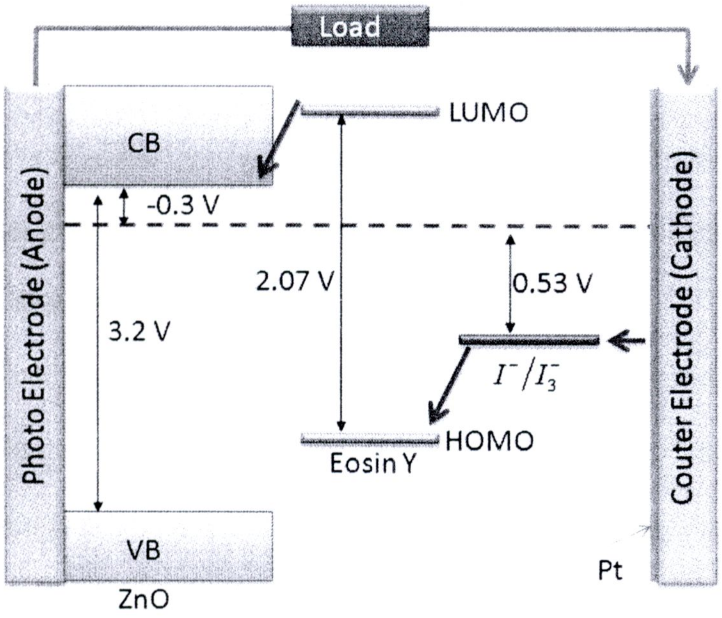

Figure 2.15 The DSSCs mechanism for generating electric power.[90]

The charge separation in the DSSCs does not depend on a build-in electrical field, but mainly relies on a competition between forward and backward electron transfer kinetics at the semiconductor/dye/electrolyte interface. The electron injection rate for the excited dye into the conduction band of TiO_2 was found to be in the nanosecond region. The backward electron transfer from the conduction band of the semiconductor to the oxidized dye was found to strongly depend on applied potential. The backward electron transfer between conduction band electron and triiodide has been found to occur in the millisecond time regime. The redox couple of the electrolyte (I^-/I_3^-) should be aligned so that there is a "downhill pathway" for the electron transport in the closed circuit, i.e. the reaction path is thermodynamically self-sustainable.

The original state of the dye is subsequently restored by electron donation from the hole conductor electrolyte. The regeneration of the sensitizer by the hole conductor intercepts the recapture of the conduction band electron by the oxidized dye. The hole conductor is regenerated in turn at the counter-electrode, and the circuit is completed via electron migration through the external load. The efficiency of solar cells devices is determined by the generation of excitons, and the dissociation and transport of the free charge carriers to the collection electrode. [92,105]

Dye sensitized solar cells (DSSCs) have attracted much attention since the initial report of O'Regan and Grätzel on realization of high efficiency at low cost. Central to the DSSCs is a thick layer of crystalline nanoparticle TiO_2/ZnO layer (5-20μm), on which a light absorbing dye/pigment/organometallic complex is anchored. This complex contacts with a redox electrolyte and Pt is used as the electrode. Dye-sensitized TiO_2 nanoparticle films have been at the forefront of research, and photon conversion efficiency of 10.4 % has been demonstrated. [93,100] However, nanoparticles based DSSCs rely on trap-limited diffusion for electron transport, a slow mechanism that can limit electron extraction efficiency. ZnO nanowires can be grown on various substrates. These nanowires have an average diameter of several tens of nanometers and a length of up to tens of micrometers, resulting in a high aspect ratio, thus providing large surface areas for anchoring the dye molecules, and meanwhile acting as the direct conducting pathways for the photo induced electrons. J. Qiu et al. have reported ZnO nanowire-based DSSCs with a full Sun power efficiency of 1.5%. [93] The FTO substrate was first covered with a thin layer of ZnO nanoparticles as the seed layer. ZnO nanowires were grown on FTO substrates from aqueous solutions containing 25 mM zinc nitrate hydrate and polyethylenimine. The ZnO nanowire arrays are first sensitized in a solution (0.5 mM l–1) of $(Bu_4N)_2Ru(dcbpyH)_2(NCS)_2$ (RuN3 dye) in dry ethanol for one hour and then sandwiched together and bonded with thermally platimzed FTO counter electrodes separated by a gasket (surlyn). The internal space of the nanowires was filled with a liquid electrolyte (0.5 M LiI, 50 mM I2, 0.5 M 4-tertbutylpyridine in 3-methoxypropionitrile) by capillary action. ZnO nanowires with a dendritic structure grown by CVD have also been used to construct DSSCs. [46-47] The dendritic ZnO nanostructures were grown from zinc acetylacetonate hydrate ($Zn(C_5H_7O_2)_2{\cdot}xH_2O$) and oxygen by multiple steps. ZnO nanowires with 100 nm diameters nucleate spontaneously on top of a thin polycrystalline ZnO film that deposits on FTO substrate during the initial stages of growth. Dye was loaded by attaching the dye to the nanowire surface in 1.0 mM aqueous KOH solution. It was found that the product of charge injection and collection efficiencies is approximately 70%. This high internal quantum efficiency confirms that the main reason for the lower current density from nanowire-based cells compared to ZnO nanoparticle-based cells is the low light harvesting efficiency. The DSSCs exhibited energy conversion efficiencies of 0.5%.

2.4 J-V measurement

The most common and important technique for solar cell is to measure the current density-voltage (J-V) curve. The photoelectrochemical characteristics of DSSCs were tested under simulated sunlight AM 1.5 came from a solar simulator with the radiant power usually of 100 mW/cm^2. The incident light intensity was calibrated with a standard Si solar cell. J-V characteristic were measured with a dc voltage and current source which interfaced and controlled by a computer. The short current density (J_{sc}), open circuit voltage (V_{oc}), fill factor (*ff*) and the overall photoconversion efficiency (η) were determined from the measured J-V curves.

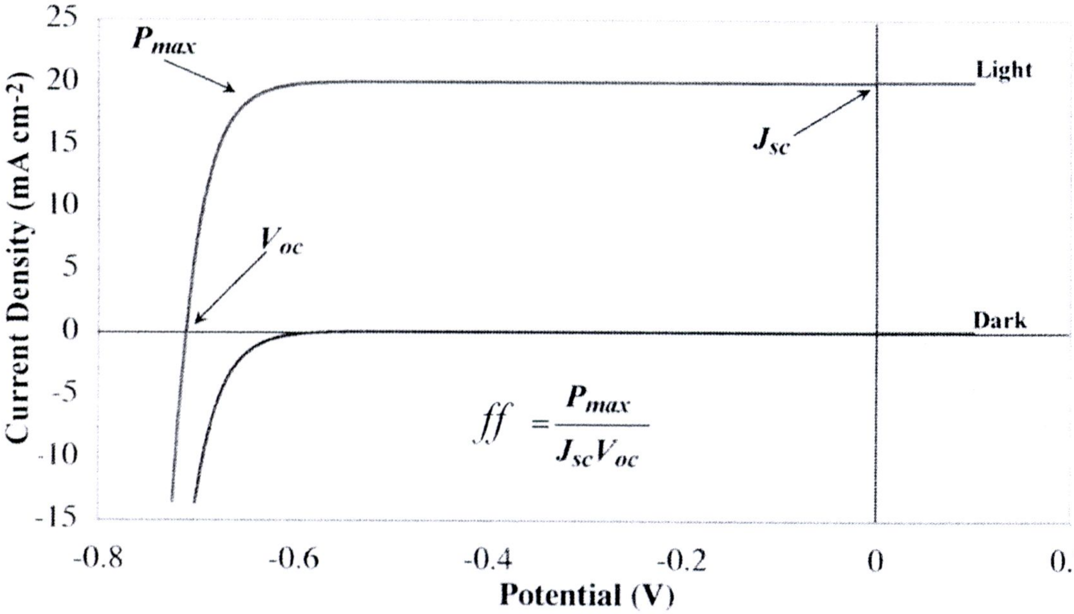

Figure 2.16 The current density-voltage curve. In this, point of maximum output power is found.

Figure 2.16 is shown a J_{sc} and V_{oc} as show in, and also a maximum output power (P_{max}) will appear. The fill factor (*ff*) is defined by

$$ff = \frac{P_{\max}}{J_{sc}V_{oc}} \tag{2.49}$$

And the ratio between the maximum output power and the input power (P_{in}), gives the efficiency (η) of DSSCs, and given by

$$\eta = \frac{P_{\max}}{P_{in}} = \frac{J_{sc}V_{oc}}{P_{in}} \times FF \tag{2.50}$$

2.5 Dielectric heating with microwave energy [54,64-65]

Contrary to convective heating with steam and hot-air, or even radiation heating in general, dielectric heating generates heat directly inside the exposed material. The conversion of electric energy to heat results from the dielectric losses of the electric non-conducting material, which is usually also a poor thermal conductor. In convective heating of materials with poor thermal conductance properties, the surface has to acquire high temperatures so that the temperature gradient, i.e., the transport of heat, will be as high as possible and account for the material's rapid heating.

Dielectric heating depends on the interaction between polar groups in molecules of non-conductive materials and the alternating electric field of electromagnetic oscillation. The atomic carriers of charges prevailing in fluid and solid materials are not able to move upon imposing an electric field E, instead, they may only be slightly dislodged from their initial position. The effective force is proportional to the electric field strength, and due to this displacement, negative and positive surface charges arise at the terminal sites. This phenomenon is referred to as polarization P and is related to the electric field by the following equation:

2.5.1 Dielectric heating [54]

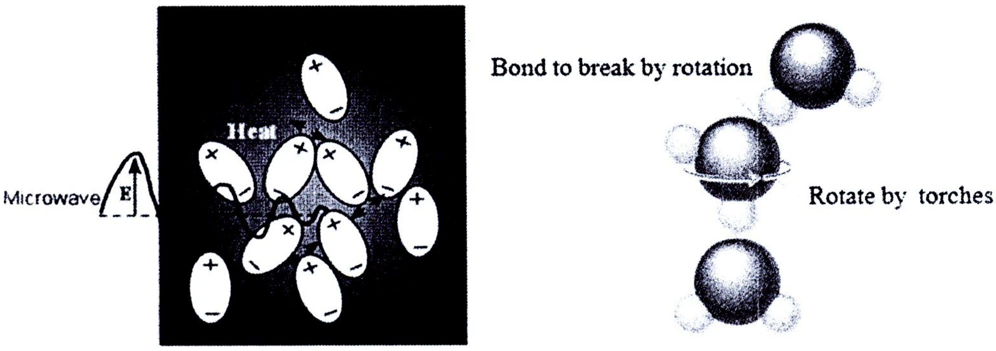

(a)

(b)

Figure 2.17 (a) Dipole rotations of molecule occurs in materials containing polar molecules having an electrical dipole moment, which will align molecules in a microwave electromagnetic field. (b) Molecular rotation for the generation of energy in the form of microwave electromagnetic radiation.

Dielectric heating (also known as electronic heating, Radio frequency (RF) heating, high-frequency heating) is the process in which radio wave or microwaveelectromagnetic radiation heats a dielectric material. This heating is caused by dipole rotation. Molecular rotation occurs in materials containing polar molecules having an electrical dipole moment, which will align molecules in an electromagnetic field, as shown in Figure 2.17(a). If the field is oscillating, as an electromagnetic wave, these molecules rotate to continuously align with it, called dipole rotation. As the field alternates, the molecules will be induced to reverse their direction accordingly. Rotating molecules push, pull, and collide with other molecules (through electrical and gravitational forces), distributing the energy to adjacent molecules and atoms in the material as shown in Figure 2.17(b).

Temperature is related to the average kinetic energy (energy of motion) of the atoms or molecules in the material - agitating the molecules in this way by the definitive increase of the temperature of the material. Dipole rotation is a mechanism by which energy in the form of electromagnetic radiation is converted to heat energy. There are other mechanisms by which this conversion occurs as well.

Dipole rotation is the mechanism normally referred to as dielectric heating, and is most widely observable in the microwave oven. It operates most efficiently on liquid water, and much less for on fats, sugars, and frozen water, because fats and sugars being far less polar than water molecules, and thus less affected by the forces generated by the alternating electromagnetic field. On the other hand, frozen water molecules are fixed in place in a crystal lattice and are not free to rotate, thus they cannot accelerate as much in response to the electromagnetic forces they experience in the external electromagnetic wave. Outside of cooking, the effect can be used to heat solids, liquids, or gases, provided that they contain some electric dipoles.

Not all materials are equally suitable for dielectric heating. The ease with which a dielectric material can be heated is represented by what is known as the loss factor: The higher the loss factor, the more energy can be absorbed in the material. The name 'loss factor' is derived from electrical engineering and is actually misleading. In electrical engineering, you want capacitors to have a low loss factor (i.e. little internal dissipation).

For dielectric heating, a high loss factor is actually a favourable property. As stated earlier, two phenomena play a role in the dielectric heating of a material: 1) the polarisation and 2) the 'rubbing' between the polarised molecules. Both elements are contained in the definition of the loss factor ε''.

$$\varepsilon'' = \varepsilon'.\tan(\delta) \qquad (2.51)$$

ε' is the relative permittivity or dielectric constant of the material. It is a direct measure of the extent to which the material can be polarised.

δ is the loss angle and is directly linked to the phase shift between the orientation of the molecules and the changing electrical field as the result of rubbing.

The power that is dissipated in a dielectric material is given by the following formula:

$$P = 2\pi.f.\varepsilon_0.(\varepsilon'.\tan(\delta)).E^2 \qquad [\mathrm{W/m^3}] \qquad (2.52)$$

f is the frequency of the electrical field [Hz]

ε_0 is the dielectric constant of vacuum ($8.84\text{x}10^{-12}$ F/m)

$\varepsilon'.\tan(\delta)$ is the loss factor of the material

E is the electrical field strength in the material [V/m]

The above formula only applies strictly to a simple arrangement with two flat plates or for an infinitesimally small volume in the dielectric material. However, in many cases the formula gives a good approximation to the dissipated power, and can be used as an estimate when conducting tests. The formula shows which elements determine the dissipated power: the frequency, the material (i.e. the dielectric properties) and the electrical field strength.

2.5.2 Effect of the loss factor

The dissipated power increases in proportion to the loss factor. In the previous paragraph it has already been mentioned that the loss factor is dependent on a number of variables such as the frequency of the electrical field, the temperature, the moisture content, etc. Temperature and degree of humidity are the properties that change most during the heating process and the associated variation in the loss factor can dramatically affect the process. With increasing temperature, the loss factor will often increase. A material whose loss factor has a positive temperature coefficient (figure 1a) will, from a critical temperature T_c, suddenly start to dissipate much more energy, generally at the hottest places. The effect is known as thermal runaway and can damage the product. Critical temperatures often arise around

THE NATIONAL RESEARCH COUNCIL OF THAILAND
RESEARCH LIBRARY

2.5.3 Penetration depth

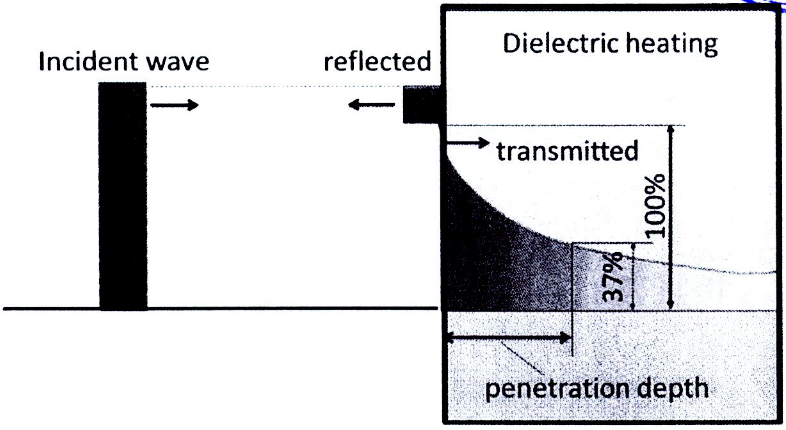

Figure 2.18 Power flow when an electromagnetic wave strikes a dielectric material with high loss factor

Generally stated, the penetration depth is smaller for microwave heating because the frequency is many times higher than in radio frequency installations. However the dielectric properties of the material that is to be heated also play a major role. When electromagnetic radiation strikes an object, part of the radiation will be reflected. The remaining part penetrates into the material and is gradually absorbed.

The gradual absorption of power is characterized by the penetration depth d. This is defined as the depth in the material at which the transferred power has been reduced to 37% of its original value. To put it another way: 63% of the transferred power is dissipated in a surface layer of thickness, *d*. The penetration depth is inversely proportional to the frequency, tan(*d*) and the root of the relative permittivity:

In the natural sciences, the term diathermy means "electrically induced heat" and is commonly used for muscle relaxation. It is one of the methods of heating tissue electromagnetically or ultrasonically for therapeutic purposes in medicine. Ultrasonic diathermy refers to heating of tissues by ultrasound for the purpose of therapeutic deep heating. No tissue is ordinarily damaged hence it is generally used in biomedical applications. Electric diathermy uses high frequency alternating electric or magnetic fields, sometimes with no electrode or device contact to the skin, to induce gentle deep tissue heating by induction or dipole rotation.

2.5.4 Microwave plasma

The most widely used method for plasma generation utilizes the electrical breakdown of a neutral gas in the presence of an external electric field. Charge carriers accelerated in the electric field couple their energy into the plasma via collisions with other particles. Electrons retain most of their energy in elastic collisions with atoms and molecules because of their small mass and transfer their energy primarily in inelastic collisions. Discharges are classified as dc discharges, ac discharges, or pulsed discharges on the basis of the temporal behaviour of the sustaining electric field. The spatial and temporal characteristics of a plasma depend to a large degree on the particular application for which the plasma will be used.

2.5.5 RF and microwave discharges [62]

Discharges excited and sustained by high-frequency electromagnetic fields are of increasing interest for technical and industrial applications. The power absorption P_{abs} per volume V by a plasma in a high-frequency field is given by

$$\frac{P_{abs}}{V} = \frac{1}{2} n_e \frac{e^2}{m_e \nu} \frac{\nu^2}{\nu^2 + \omega^2} E_0^2 \tag{2.53}$$

where n_e is the electron density, e and me are the electron charge and mass, ν is the electron–neutral collision frequency, and ω refers to the angular frequency of the electromagnetic field whose amplitude is E_0. In the presence of a magnetic field B perpendicular to the electric field, the power absorption changes to

$$\frac{P_{abs}}{V} = \frac{1}{4} \frac{e^2}{m\nu} \left(\frac{\nu^2}{\nu^2 + (\omega - \omega_c)^2} + \frac{\nu^2}{\nu^2 + (\omega + \omega_c)^2} \right) E_0^2 \tag{2.54}$$

where ω_c denotes the electron cyclotron frequency. Electromagnetic waves with frequencies below the electron plasma frequency

$$\omega_c = \left(\frac{e_0^2 n_e}{\varepsilon_0 m_e} \right)^{1/2} \tag{2.55}$$

(here ε_0 denotes the permittivity of vacuum) will be reflected. Therefore, the electron density corresponding to the electron plasma frequency is called the cut-off density.

However, the skin effect enables the penetration of the wave into the plasma to some extent. The power absorption is limited to the dimension of the skin sheath of thickness δ_s .For $\nu >> \omega$ the skin depth is given by

$$\delta_s = \sqrt{2}c\left(\frac{\varepsilon_0 m_e \nu}{e^2 n_e \omega}\right)^{1/2} \tag{2.56}$$

In a non-thermal plasma with ne = 10^{10} cm^{-3} and $\nu = 10^9$ s^{-1} the above relation yields a skin depth of 0.25 m and 0.02 m, respectively, for frequencies of 13.56 MHz and 2.45 GHz. Rf discharges usually operate in the frequency range $f = \omega / 2\pi \cong 1 - 100 MHz$. The corresponding wavelengths (λ = 300–3 m) are large compared to the dimensions of the plasma reactor. For microwaves the most commonly used wavelength is 12.24 cm, corresponding to a frequency of 2.45 GHz. This wavelength is roughly comparable to the dimensions of a typical microwave reactor. For lower frequencies, the ions accelerated in the field move towards the electrodes and produce secondary electrons, similar to what happens in a dc discharge. As the frequency increases, the ions and subsequently also the electrons can no longer reach the electrode surface during the acceleration phase of the exciting external field.

Plasma generation using microwaves is widely employed in many applications [55-64]. Characteristic features of microwaves are the wavelength, which is comparable to the dimensions of the plasma apparatus (2.45 GHz: λ =12.24 cm), and the short period of the exciting microwave field. The amplitude of the oscillations of the electrons in the microwave field is very small. For an excitation frequency f = 2.45 GHz and an amplitude E_0 = 500 V cm^{-1} it is 3.5×10^{-3} cm. The power absorption (equation (2.53)) depends on the electron–neutral collision frequency, i.e. on the gas pressure and the gas composition. The absorption efficiency in a 2.45 GHz discharge is high for He in the region between 10^3 and 10^4 Pa, whereas the maximum efficiency for Ar is reached for 200 Pa. However, microwave discharges can be operated at higher pressures as well, even at atmospheric pressure. The corresponding cut-off density of the electrons at 2.45 GHz is about 10^{11} cm^{-3}. Waves of this frequency can penetrate into plasmas with higher densities only up to the thickness of the skin sheath (equation (2.56)), which equals a few centimetres under these conditions. The microwave power absorption inside the skin sheath transfers energy into the plasma via waves with a frequency below the cut-off frequency. A microwave plasma reactor consists in principle of a microwave power supply, a circulator, the applicator, and the plasma load. The transmission lines are rectangular waveguides or, at lower powers, coaxial cables. The applicator should optimize the energy transfer into the plasma and minimize the power reflection. The circulator protects the power supply from reflected power.

2.5.6 Microwave plasma source (Deachana, 2009)

The plasma-assisted material process has wide application by various plasma sources for deposition, etching and cleaning on various surfaces. The main burden was carried by capacitively and inductively coupled RF (mainly 13.56 MHz) plasmas. The rational for excluding the microwave plasmas was that microwaves have limited penetration, e.g., microwave plasmas cannot penetrate into high-density non-magnetized plasmas (plasmas of density higher than the cut-off density $n_c = \varepsilon_0 m_c \omega^2 / q^2$ which is $n_c = 7.4 \times 10^{10} cm^{-3}$ for ω/2π GHz), they can interact with the plasma only as surface waves propagating along the plasma boundary, and such waves can propagate only if the boundary faces a dielectric. Plasmas sustained by such waves are referred to as surface-wave plasmas.

2.5.7 Generation of a plasma by microwave

The working gas is the principal mechanism of creating a plasma by collision between electrons and neutral particles. To ionize a gas atom/molecule sufficient energy, ionization energy, is required. This can be obtained by accelerating electrons by electric fields. For a DC discharge, electrons are generated from a hot filament and are accelerated to the chamber wall. The potential required to accelerate those electrons is usually larger than the ionization energy of the working gas atom/molecule. As electrons travel through the gas they gain energy from the electric fields and at some point they collide with the ambient gas. Electrons whose energy exceed ionization energy are able to ionize the gas atom/molecule. Those whose energy is less than the ionization energy would excite the atoms/molecules. The excited atoms/molecules emit electromagnetic wave as they proceed back to ground state. This is why we usually see that plasmas are glowing. However, for microwave frequencies electrons are shaken by the oscillating fields and can move only few μm during a period of the wave. Without collision electrons could never gain enough energy to ionize atoms/molecules. Elastic collision between electrons and the heavy particles is essential for electrons to gain energy. Statistically, it is possible that some electrons collide with the heavy particle every half period of the applied fields and gain sufficient energy to ionize the gas. After giving energy to the atoms/molecules the energy-gaining process is repeated over and over. The mean power transfer per electron θ_A is given by

$$\theta_A = \frac{e^2}{m_e} \frac{\nu_e}{\nu_e^2 + \omega^2} E_{rms}^2 \tag{2.57}$$

It is the average work done by the electric field by unit time. Where θ_A is the mean power transfer per electron. ν_e is the electron-heavy particle collision frequency. ω is the applied microwave angular frequency. E_{rms} is the root-mean-square electric field.

At zero collision frequencies there is no collision and there is no chance that electrons collides with heavy particles. In this case, electrons are just oscillating with a magnitude of few micrometer. The energy transfer is zero and the plasma is not generated. This is referred to as the vacuum insulation. At very high collision frequencies-high pressure-electrons collide too many times during a period of the applied fields, resulting in a small amount of energy transfer. This is called the high pressure insulation. The power transfer can be enhanced by controlling the pressure of the discharge chamber so that the collision frequency is equal to the field applicator frequency.

Radio frequency and microwave heating are electroheat techniques that are applied for heating materials that are poor electrical conductors. Often, they are also poor conductors of heat. In general these materials are known as dielectric materials or dielectrics. When a dielectric material is brought into a rapidly altering electrical field, heat is generated inside the material. This is known as heating by dielectric hysteresis or, in short, dielectric heating. Radio frequency and microwave heating are both applications of this principle. In technological terms, however, there is a clear distinction between the two techniques. The essential advantage of dielectric heating resides in the generation of heat within the material to be heated. In comparison with more conventional heating techniques (hot air, infrared) in which the material is heated via the outer surface, dielectric heating is much more rapid. This is because electrically insulating materials are mostly also poor conductors of heat.

Houmes et al. (1996) prepared recently a number of nitrides such as TiN, AlN, and GaN by the use of a plasma by exposing oxides to plasma of N_2/H_2 [55].

Houmes et al.(1997) reported microwave-assisted synthesis of binary (TiN, AlN, and VN) and ternary (Li_3FeN_2, Li_3TiN_2, Li_3AlN_2) nitrides by a direct reaction between metal powder and nitrogen by first striking a N_2 plasma for a low power microwave source as shown in Figure 2.19. Ternary nitrides were produced by direct reaction of either the component nitrides or a mixture of Li_3N and metal powder reacted in nitrogen plasma. It was noted that sustaining a plasma in the domestic microwave oven is unfeasible. Microwave-generated N_2 plasma reactions were also used to demonstrate the formation of Si_3N_4 and BN [55].

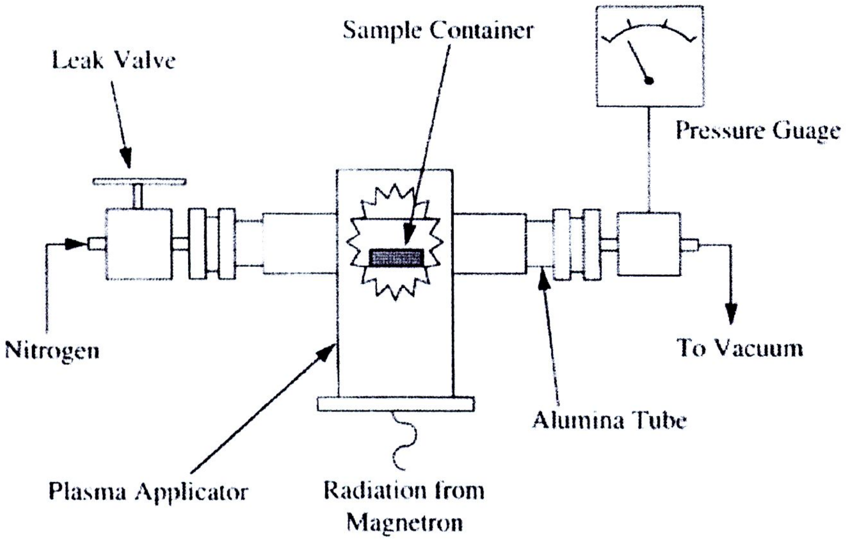

Figure 2.19 Schematic diagram of Cober microwave system used in the synthesis of binary nitride materials by exposing in a nitrogen plasma [55].

Douthwaite et al. (1996) reported a rapid synthesis of alkali metal fullerides by using microwave induced argon plasma. Reaction times appear to be only a few seconds while the conventional preparation takes a longer time. The microwave plasma was generated in argon held at a pressure of 1-0.5 kPa in evacuated quartz tubes. Fullerenes and alkali metals are kept physically separated, and the tube was at the position that the microwave amplitude was at the highest. The alkali metal quickly heated and vaporized, and the C_{60} reacted with condensed K under the Ar plasma. Under these conditions, K intercalated easily. It was also confirmed that uncondensed K in the plasma was not able to intercalate. It has been shown by alteration of reaction conditions that there was a thermal action of the plasma which was responsible for the rapid synthesis [59].

Cho et al. (2008) presented a microwave plasma torch system to a low-pressure chamber. The electric field induced in a quartz discharge tube by microwave radiation breaks down the gas at a sufficiently low pressure, igniting the plasma, which is continuously sustained by microwave radiation. The plasma profile at a very low pressure is shown to be asymmetric with higher density on the incoming side of the microwave. The plasma density increases as the microwave power increase. The typical argon plasma density of a plasma torch powered at 500 W under a pressure of 19.99 kPa is on the order of $10^{14}/cm^3$. The electron temperature in the argon torch plasma was estimated to be 1.5 eV, thereby effectively exciting the molecules in the torch gas. Disintegration of nitrogen fluoride (NF_3) indicates that a microwave plasma torch operating at a low pressure can efficiently generate an abundant amount of chemical radicals [34].

Hong et al. (2005) have directly synthesized the N-doped titanium dioxide (TiO_2) particles of nanosize in an atmospheric microwave plasma-torch using gas-phase titanium tetrachloride ($TiCl_4$) [97].

Douthwaite et al. (2008) reported the rapid synthesis of alkali metal fullerides using a microwave induced argon plasma (MIAP). Reaction times are of the order of seconds using a MIAP, but conventional synthesis requires times of the order of several days [36].

Wu et al. (2000) presented the results of new 160-mm homogeneous plasmas produced at the pressure of 10-600 Pa. Homogeneous microwave plasmas have been produced and used for materials surface modification. Also, the axial distributions of plasma parameters have been investigated, with and without the short circuit at the top of the set-up, respectively. The experimental results showed that the short circuit was efficient for the plasma density being raised and beneficial for plasma uniformity [99].

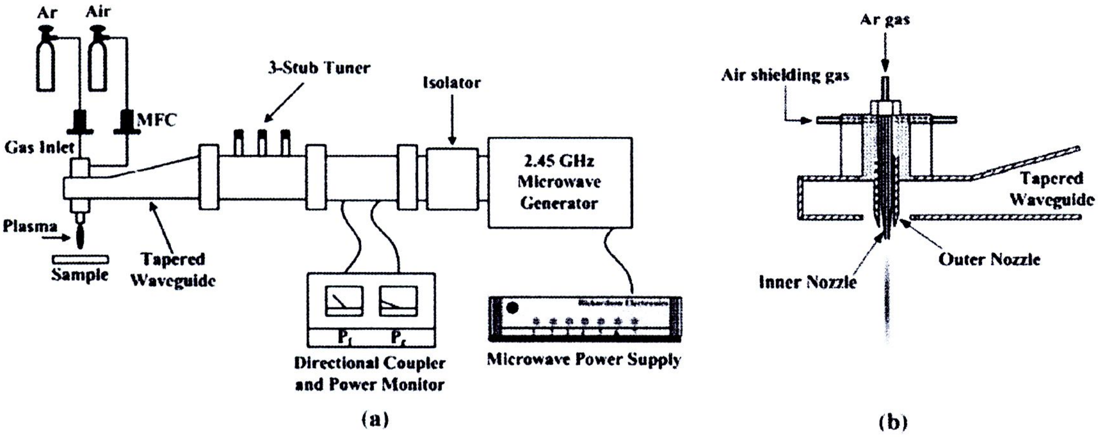

Figure 2.20 Schematic diagram of (a) the apparatus for plasma modification by making use of an atmospheric microwave plasma torch, and (b) the construction of the plasma nozzles [58]1

Shin et al. (2007) presented continuous wave (CW) microwave discharges to operate at atmospheric pressure in argon gas, which were applied to surface modification of metal surfaces for improvement of adhesion with pain coating as shown in Figure 2.20.

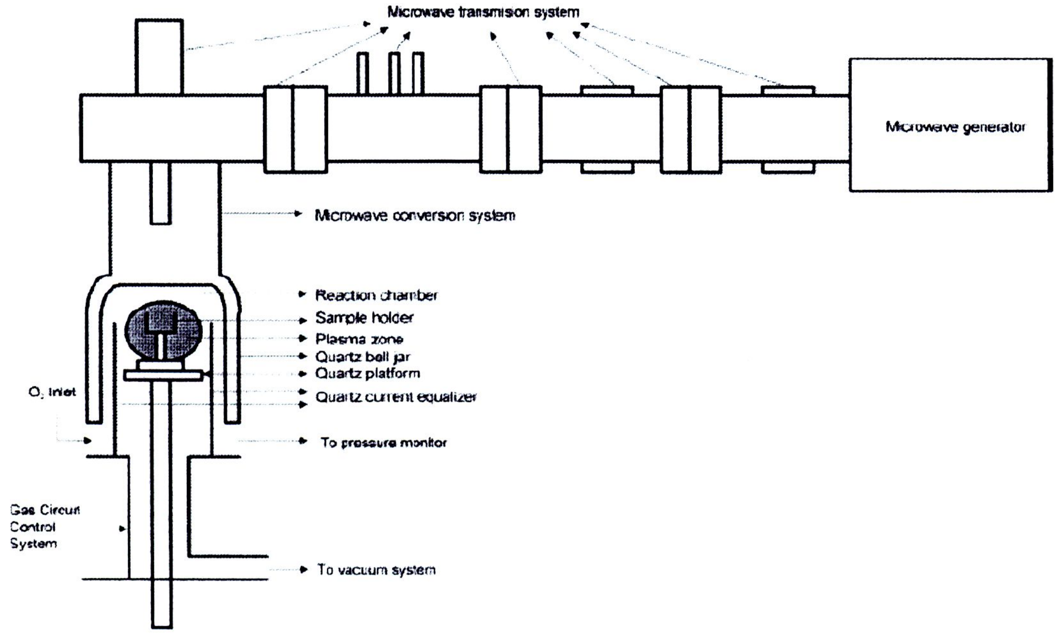

Figure 2.21 A schematic diagram of microwave plasma equipment [58].

Zhen et al. (2007) have been synthesized the high density, nanocrystalline Bi_2O_3-HfO_2-Y_2O_3 solid electrolyte by microwave plasma and pressure-less sintering as shown in Figure 2.21. After the samples were sintered by microwave plasma at 700°C for 30 min, the relative density was found to be greater than 96%. Moreover, the sintered specimens exhibit considerably finer microstructure and denser, compared to that of the samples sintered by a conventional pressure-less condition.

2.6 Properties and synthesis of cadmium sulfide (CdS)

Cadmium sulfide (CdS) has, like zinc sulfide, two crystal forms; the more stable hexagonal wurtzite structure (found in the mineral Greenockite) and the cubic zinc blende structure (found in the mineral Hawleyite). In both of these forms the cadmium and sulfur atoms are four coordinate.

CdS is one of the most important II–IV group semiconductors, which are extensively applied in optical and electronic fields such as biological labeling, light-emitting diodes, and photoelectric conversion devices, solar cells, photocatalysis and environmental sensor, it is a direct band gap material with Eg = 2.50 eV.

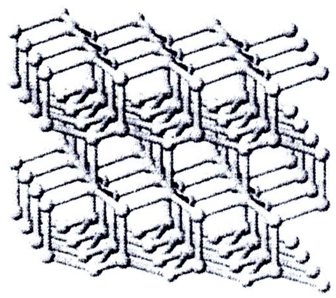

Properties		Structure	
Molecular formula	CdS	Crystal structure	Wurtzite (hex.)
Molecular mass	144.47 g mol	Lattice constant	a.b = 4.135 Å c = 6.749 Å
Appearance	Yellow-red solid	**Effective mass (m*)**	
Density	4.87 g cm^{-3}	m_e*	0.21
Melting point	2023 K	m_h*	0.80
Band gap (300K)	2.50 eV (direct)		
Electron affinity	4.79 eV		

Figure 2.22 The properties and structure of CdS (wurtzite) [71]

Preparation of CdS nanorods is an attractive research area. A novel route of thermal decomposition of a single-source precursor in a monosurfactant system has been suggested to grow CdS nanorods with controlled size and shape (such as mono-, bi-, tri- and tetrapods) by varying the reaction temperature and concentration of the precursor. Ye et al. [95] have synthesized CdS nanowires by the vapor–solid synthetic route with different morphologies with a controlled heating duration. In the evaporation–condensation method, CdS powder was evaporated at a temperature of 800–1000 °C to grow nanorods by vapor–solid mechanism. While the shape control of CdS was achieved by changing the growth temperature or precursor concentration [23], the size control was achieved using templates which can be organic, inorganic [39] or biological [40]. Many of the methods for the preparation of CdS nanorods are complicated; requiring high temperature or various types of templates whose preparation involves tedious procedures or complicated chemistry.

Murugan et al. [99] have prepared the nanocrystalline CdS via novel microwave–solvothermal techniques by using cadmium salt ($CdSO_4 \cdot 8/3H_2O$) and thiourea as reactants in several different solvents at low temperature (95–150°C) and short time (30 min–6 h) by irradiation of microwaves. The XRD patterns indicated that the product obtained using ($CdSO_4 \cdot 8/3H_2O$) as cadmium source with H_2O, ethylene dimine (en) and ethylene glycol (EG) as solvents is pure hexagonal CdS, respectively. Whereas the XRD pattern of the product obtained in EtOH is nearly pure hexagonal but contains may be small amount of cubic CdS. It is found that the morphology of the product is quite different. All CdS powders obtained in water (H2O) and EG display the rod-like morphology. By contrast, the CdS powders obtained in solvents such ethylene diamine and EtOH display the spherical morphology.

Dongre et al. [22] have prepared CdS nanowire by chemical bath deposition method. Nanocrystalline thin flims of CdS have been grown onto substrates and converted into nanowire (NW) networks using chemical etching process. Optical transmission spectra showed that the transmission increased when nanoparticles transferred into nanowire having band gap value 2.48 and 2.58 eV for nanoparticles and nanowires, respectively.

Quiebras et al. [23] have prepared CdS films of different thicknesses, deposited by chemical bath deposition (CBD) from a bath containing CdCl2, NH3, ammonium hydroxide and thiourea in suitable proportions. These preparations maintained under constant stirring at a temperature of 75°C during the deposition. The thickness of the films was controlled by the deposition time and the concentration of the bath. The transmission spectrum of a CBD-CdS sample sharp absorption edge at about 450nm which corresponds to a band gap of approximately 2.47 eV.

Ramaiah et al. [24] have studied structural and optical properties of as-deposited CdS films and annealed CdS films which prepared by chemical bath depositon (CBD) technique. The composition of the films was found to have a Cd to S ratio of 1:0.93, eventhough the starting solution composition (Cd:S) was maintained at 1:5. The as-grown CdS films exhibited an hexagonal structure no secondary or mixed phases were observed. However, on annealing with laser beam, the films showed both cubic and hexagonal phases. Transmission spectroscopy measurements yielded a band gap value of 2.4 eV (hexagonal phases) for as-deposited films, whereas for annealed films, the band gaps were 2.62 eV (hexagonal phases) and 2.35 eV (cubic phases). This indicates that the annealed films showed higher band gap value compared to that of as-grown films.

Perez et al. [25] have prepared CdSe thin films by chemical bath deposition (CBD) and pulsed laser deposition (PLD) methods. For CBD films, cadmium chloride ($CdCl_2$) and cadmium acetate ($Cd(CH_3COO)_2$) solutions were employed as Cd^{2+} source while a freshly prepared sodium selenosulfite (Na_2SeSO_3) solution provided the Se^{2-} ions. The pH of the bath was adjusted by adding ammonium hydroxide. The effects of the bath temperatures (30–90°C) and the Cd/Se ratio on film properties were investigated. On the other hand, PLD films were grown by the ablation of a sintered pure CdSe target using a Nd:YAG laser beam (355 nm) with 1 J/cm^2 fluence. The deposition chamber was maintained under vacuum pressure (1- 0.6 kPa) at room temperature. The CBD films are constituted by crystallites of metastable cubic phase (7 nm) with some amorphous phase present, whereas the PLD films showed better crystalline quality and higher crystalline size. Optical absorption analysis shows that the band gap value of the CBD films is higher than that of the bulk material and decreases with the bath temperature. Annealing transforms the metastable cubic phase into the hexagonal phase and causes a redshift in the band gap of the CBD and PLD films due to the increase of crystal size.

Pandey et al. [26] have been prepared the growth of cadmium telluride (CdTe) thin films by pulsed laser deposition (PLD) using excimer laser (KrF, λ=248 nm, 10 Hz) on corning 7059 glass and SnO_2-coated glass (SnO_2/glass) substrates at different substrate temperatures and at different laser energy pulses. X-ray diffraction analysis confirms the formation of CdTe cubic phase at all pulse energies except at 200 mJ. At 200 mJ laser energy, the films show hexagonal phase. The band gap of CdTe films was found as 1.54 eV for hexagonal phase and ~1.6 eV for cubic phase.

Perna et al. [27] have been prepared the growth of CdS films on quartz substrate by means of pulsed laser deposition using Nd:Yag laser doubled (λ=532 nm, 10 Hz). The X-ray analysis showed that the CdS films grow in the wurtzite hexagonal phase. The absorption edge presents a red-shift with increasing temperature, due to the decrease of the band gap.

Liu et al. [28] have been successfully synthesized CdSe microstructure by modified hydrothermal method with $Cd(NO_3)_2$ and Na_2SeO_3 as precursors and hydrazine hydrate as a reductant in the presence of 1-n-butyl-3-methylimidazolium bromide ([Bmim]Br) at 140°C for 16 h. It was found that the CdSe were purity wurtzite phase. The results indicated that the CdSe microspheres have an average size of about 3 μm and were assembled by CdSe nanoparticles with size ranging from 20 to 40 nm. It was found that the pH and [Bmim]Br have influence on the morphologies of the products.

Thongtem et al. [29] have prepared CdS (hexagonal structure) with different morphologies by the reaction of cadmium chloride and thiourea in different solvents (benzene, toluene, p-xylene, cyclohexane and tetrahydrofuran). It was found that solvent polarities were play a significant role in shape and size of the final products. Photoluminescence spectra of the obtained products were blue shifted in comparison with the bulk CdS. Furthermore, they also found that photoluminescence intensity of the rod shaped crystal synthesized in tetrahydrofuran was at the highest.

Yang et al. [30] have prepared CdSe and CdTe nanowires by PVA-assited solvothermal method using ethylenediamine as a coordinating solvent. The as-prepared CdSe was mostly in zinc blend phase (little wurzite phase) and as-prepared CdTe sample was very completely zinc blend phase. In addition, they found that PVA and temperature were main factors in the formation of nanowire and the structure of CdSe and CdTe.

Kokate et al [31] have studied effect of annealing on properties of electrochemically deposited CdTe thin flims. It was found energy gap of the materials is direct type with band gap energy 1.64 eV and after annealing it decreases to 1.50 eV.

Bhunia et al [33] have synthesized ZnTe by microwave synthesis using high purity Zn and Te and the minimum reaction time determined to be 30 min. The materials in powder form were placed in silica tube and evacuated to a pressure of 1.33 kPa and sealed which was placed in a conventional microwave oven having a power rating of 900W operating at 2.45 GHz. The results indicated good crystal quality of CdS.

Suriwong et al. [34] have succesfull synthesized cubic ZnTe nanocrystals. Zn and Te powders were mixted with 1:1 and 1.8:1 molar ratios of Zn:Te and using a 900W microwave plasma under 4.3±1 kPa argon absolute pressure. No such impurities were detected, when the experimental time length was optimized. Morphologies of molar ratio 1:1 and 1.8:1 were composed of 73.37 nm facet nanoparticles with different orientations and composed of a number of irregular nanoparticles in clusters, respectively.

He et al. [35] have prepared monodispersed PVP-capped ZnS and CdS nanocrytals by microwave irradiation method. It was found that both ZnS and CdS were high purity cubic phase. Photoluminescence spectra of CdS and ZnS nanoparticles showed a narrow and broad peak, respectively. The results indicated that the narrow size distribution and goodcrystal quality of CdS whereas a broad peak of ZnS attributed to emission from surface traps. The difference of absorption spectra and product morphology of same reaction condition indicated that microwave irradiation could selectively influence the nuecleation and growth rates of different semiconductor nanoparticles.

Lerma et al. [36] have been prepared CdTe coatings by the reaction between films of cadmium hydroxide deposited on glass and a solution prepared by the dissolution of tellurium in hydroxymethane sulfinic acid. The CdTe obtained was cubic, has the absorption edge is placed at a wavelength of 818 nm corresponds to a band gap of 1.51 eV, but does not display high photosensitivity.

Sun et al. [39] have successfully synthesized CdS nanoparticles and nanorods via a solvothermal method combined with ultrasonic treatment. Cadmium chloride and thioacetamide were selected as starting materials, water and n-haptane as a solvent. It was found that treatment temperature and heating time were the major variables to control the crystal phase, size and morphology of CdS nanocrystalline.The crystal structure of CdS was completely transformed from cubic to hexagonal structure at 150°C for 1.5 h. As the temperature and time were increased, the particle size of CdS was increased and its morphologies varied from spherical to rod shape. In addition, this effect can promote the red shift of fluorescence emission of the sample.

Zhang et al. [41] have prepared CdS nanorods in microemulsions formed by nonionic surfactant TX-100 and cosurfactant hexanol with cadmium chloride and thiourea as the cadmium and sulfur sources, respectively. It was found that the obtained CdS nanorods were very uniform with their sized of 15-30 nm in diameter and 40-300 nm in legth depending on the reaction condition, for example concentration of reactants, water content, types of cadmium salt and acidic media, temperature and composition of the microemulsions.

2.7 Properties and synthesis of cadmium telluride (CdTe)

Cadmium telluride (CdTe) is a crystalline compound formed from cadmium and tellurium. It is used as an infrared optical window and a solar cell material. It is usually sandwiched with cadmium sulfide to form a p-n junction photovoltaic solar cell. Typically, CdTe cells use a n-i-p structure.

CdTe is used as an infrared optical material for optical windows and lenses but it has small application and is limited by its toxicity such that few optical houses will consider working with it. An early form of CdTe for IR use was marketed under the trademarked name of Irtran-6 but this is obsolete.

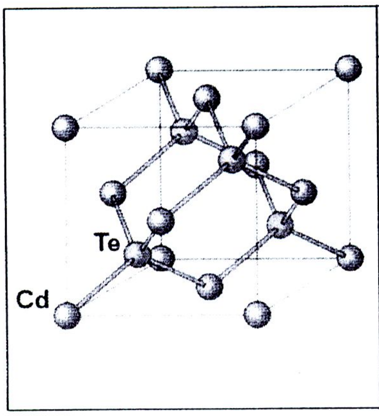

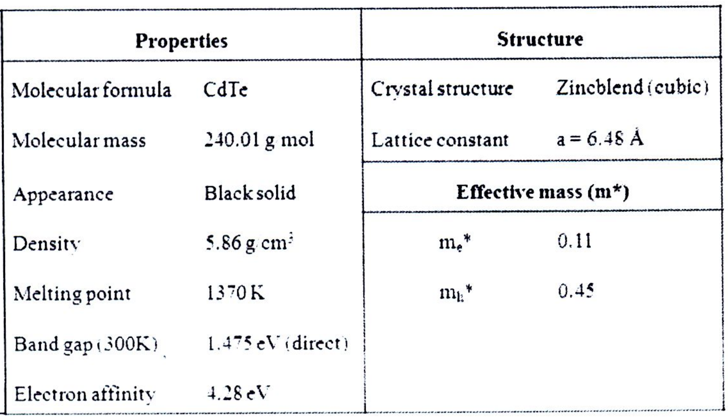

Properties		Structure	
Molecular formula	CdTe	Crystal structure	Zincblend (cubic)
Molecular mass	240.01 g/mol	Lattice constant	a = 6.48 Å
Appearance	Black solid	**Effective mass (m*)**	
Density	5.86 g/cm^3	m_e^*	0.11
Melting point	1370 K	m_h^*	0.45
Band gap (300K)	1.475 eV (direct)		
Electron affinity	4.28 eV		

Figure 2.23 The properties and structure of CdTe (cubic) [72]

CdTe is a highly useful material in the making of thin film solar cells. Thin-film CdTe provides a cost-effective solar cell design and has a higher theoretical maximum efficiency than silicon cells. Higher theoretical maximum efficiency is due to CdTe's band gap being closer to the peak of the solar output spectrum. Also, CdTe cells operate better in high temperature conditions then silicon cells.

CdTe can be alloyed with mercury to make a versatile infrared detector material (HgCdTe). CdTe alloyed with a small amount of zinc makes an excellent solid-state X-ray and gamma ray detector (CdZnTe).

CdTe doped with chlorine is used as a radiation detector for x-rays, gamma rays, beta particles and alpha particles. CdTe can operate at room temperature allowing the construction of compact detectors for a wide variety of applications in nuclear spectroscopy.[72] The properties that make CdTe superior for the realization of high performance gamma- and x-ray detectors are high atomic number, large bandgap and high electron mobility ~1100 $cm^2/V{\cdot}s$, which result in high intrinsic μ_τ (mobility-lifetime) product and therefore high degree of charge collection and excellent spectral resolution.

2.8 Properties and synthesis of zinc telluride (ZnTe)

Zinc telluride is the chemical compound with the ZnTe formula. This solid is an intrinsicsemiconductor material with band gap of 2.23–2.25 eV. It is usually a p-type semiconductor. Its crystal structure is cubic (Figure 2.25), as both ofsphalerite and diamond.Its lattice constant is 0.61034 nm, allowing it to be grown with or on aluminum,antimonide, gallium antimonide, indium arsenide, and lead selenide. It has the appearance of grey or brownish-red powder, or ruby-red crystals when refined by sublimation. Zinc telluride can be prepared as hexagonal crystals (wurzite structure).

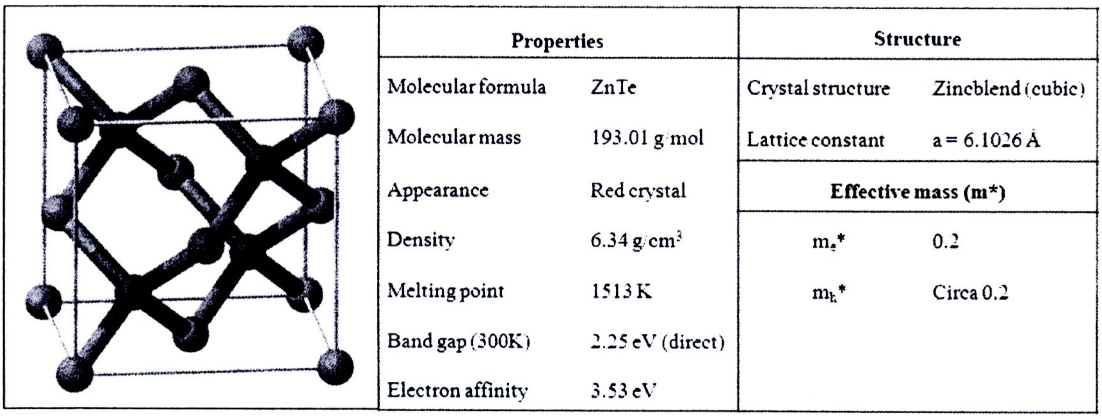

Properties		**Structure**	
Molecular formula	ZnTe	Crystal structure	Zincblend (cubic)
Molecular mass	193.01 g/mol	Lattice constant	a = 6.1026 Å
Appearance	Red crystal	**Effective mass (m*)**	
Density	6.34 g/cm^3	m_e^*	0.2
Melting point	1513 K	m_h^*	Circa 0.2
Band gap (300K)	2.25 eV (direct)		
Electron affinity	3.53 eV		

Figure 2.24 The properties and structure of ZnTe (cubic) [67]

Zinc telluride is important for development of various semiconductor devices, including blue LEDs, laser diodes, solar cells, and components of microwave generators. It can be used for solar cells as a background layer and *p*-type semiconductor in PIN structure (e.g. using cadmium telluride; *p*-type or *i*-type (intrinsic) semiconductor, and cadmium sulfide (*n*-type semiconductor). Zinc telluride together with lithium niobate is often used for generation of pulsed terahertz radiation in time-domain terahertz spectroscopy and terahertz imaging. When a crystal of such material is subjected to a high-intensity light pulse of subpicosecond duration, it emits a pulse of terahertz frequency through a nonlinear optical process called optical rectification. Conversely, subjecting a zinc telluride crystal to terahertz radiation causes it to show optical birefringence (double refraction) and change the polarization of a transmitting light, making it an electro-optic detector.

THE NATIONAL RESEARCH COUNCIL OF THAILAND
RESEARCH LIBRARY

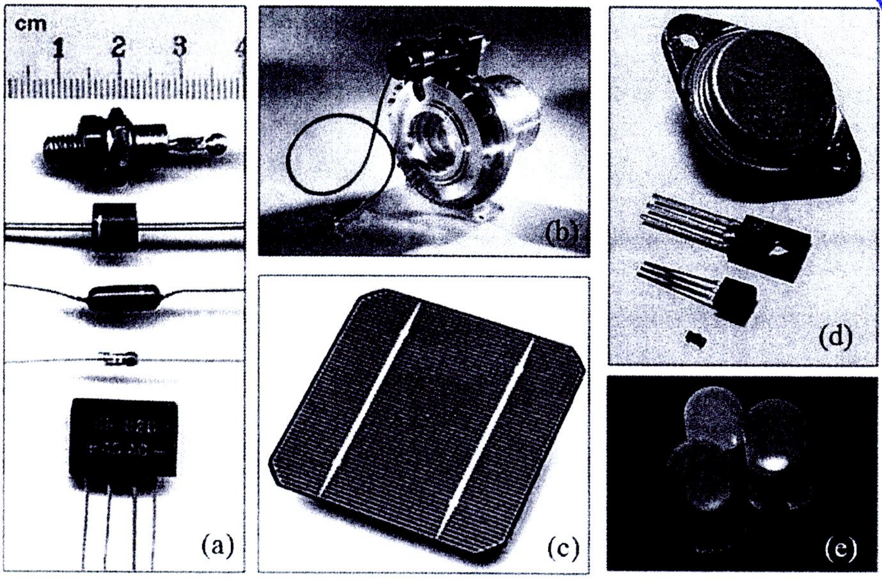

Figure 2.25 The ZnTe applications (a) semiconductor diodes, (b) electro-optics, (c) solar cells, (d) assorted discrete transistors and (e) light-emitting diodes (LED).

Bhunia and Bose (1998) have synthesized ZnTe for the first time by microwave heating from high purified Zn and Te, and the minimum reaction time determined to be 30 min. Single crystals were grown by modified vertical Bridgman technique from 4% rich Te melt, the growth direction being found to be the [111]. XRD showed formation of the zincblende phase with lattice constant 6.106 Å. Inductively coupled plasma (ICP) analysis showed Si, In, Cu, Au, and Fe to be the main impurities present at ppm level. Crystals were p-type with 8.5 Ωcm resistivity, $1.6\text{x}10^{16}$ cm^{-3}hole concentration and 46 cm^2/Vs mobility at 300 K. Mobility was found to vary with temperature as $\mu_p \propto T^{-2.7}$in the range 120-300 K. Photoluminescence (PL) at 10 K showed emission peaks at 2.06, 1.47, 1.33 and 1.05 eV. Thermal quenching of the PL bands has been studied. The samples showed weak photoconductivity due to small minority carrier lifetime. From the temperature dependence of the photoconductive gain, the minority carrier lifetime (τ_n) has been determined in the temperature range of 80-300 K. τ_n was thus found to go through a maximum of 4.5x10^{-7} s at 220 K [50].

Li et al. (2005) have synthesized semiconductor ZnTe nanowire arrays by the pulsed electrochemical deposition from aqueous solution into porous anodic alumina membranes (AAM). High-filling and ordered ZnTe nanowire arrays have been prepared from aqueous solutions by the pulsed electrochemical deposition into the pores of AAM. The ZnTe nanowires are single-crystalline and have a preferential orientation along the [110] direction. The optical absorption band edge of ZnTe nanowires exhibits a marked blue-shift compared with that of bulk ZnTe due to quantum size effect. ZnTe nanowire arrays were very interesting for applications in optoelectronic and thermoelectric nanodevices in the future [51].

Lee et al. (2007) synthesized highly crystalline zinc telluride (ZnTe) nanocrystals with a controlled shape using various growth conditions. The following amines were used as activation agents for the zinc precursor: zinc stearate, octylamine (OA), dodecylamine (DDA), octadecylamine (ODA), and trioctylamine (TOA). Unique 3-D nanoflowers (av. size= 20-120 nm), consisted of a number of nanodots (av. size = 4-11 nm) were efficiently produced when no amine or TOA was used. Dispersed nanodots were produced when OA, DDA, or ODA were used. These results indicate that the steric effect of alkyl chains plays an important role in the formation of nanoflowers. Furthermore, the shape evolution from nanoflowers to nanorods occurred at higher growth temperatures, and nanoflowers and nanorods eventually evolved into nanodots after incubation [73].

Fanfair et al. (2008) reported the synthesis of ZnE (E = S, Se, Te) nanowires in solution via the solution-liquid-solid (SLS) mechanism. Relatively low nanowire growth temperatures, between 340 and 350 °C, were made possible by using bismuth nanocrystals as seeds. Diethylzinc and zinc(oleate)$_2$ were studied as Zn reactants, and TOP:E complexes were explored as the chalcogen source. The influence of the solvent on the quality and yield of the nanowires was studied with reactions carried out in either the noncoordinating solvent squalane or the coordinating solvents, trioctylamine (TOA) or trioctylphosphine oxide (TOPO). The solvent and reactant chemistry dramatically affect the yield and quality of the nanowires, with Et$_2$Zn being more reactive than Zn(oleate)$_2$. The use of coordinating solvents provides a means to optimize nanowire growth.

Huang et al. (2008) have synthesized the submicrosizedZnE rods, ZnO/ZnE cables, and ZnE tubes (E = S, Se, Te) via exterior-to-interior boron-chalcogen corrosions on the initial ZnO rods. The morphologies of both ZnE rods and ZnO/ZnE cables are roughly comparable to that of ZnO. The measured optical gaps of the ZnE rods are in agreement with those of the corresponding bulk materials, and the ZnO/ZnE cables exhibit type-I excitonic localization that is restrained in the region of the narrower band gap component [106].

Meng et al. (2008) have synthesized zinc-blende-structured ZnTe nanostructures, periodically twinned nanowires and uniform nanoribbons,by the hydrogen-assisted thermal evaporation method in the presence of Aucatalyst via the vapor–liquid–solid (VLS) growth mechanism. The formation of various nanostructures isdependent on the local temperature. The experimental results indicate that twinned nanowires grow along the [111] direction and uniform nanoribbons grow along the [111] and [211] directions. The local temperature of ZnTe growth is the key factor to form various ZnTe nanostructures. Periodically twinned nanowires dominate in the low-temperature zone, whereas uniform nanoribbons dominate in the high-temperature zone. Besides, the transition from the twinned nanowire to the uniform nanoribbon takes place in the middle-temperature zone. EDX analysis and Raman spectrum confirm that twin boundaries are composed of excessive Te layers. Twins or excessive Te atoms cause slightly red shift of the emission in PL spectrum, which might be potentially used for nanodevices.

Guo et al. (2008) have prepared multilayer superstructures of single-crystalline ZnTe nanowire films through a new growth process: well-aligned ZnTe nanowires congregate into nanowire film. The growth process takes place discontinuously and consequently produces many layers of aligned ZnTe nanowire superstructures. These interesting findings are apparently different from the conventional vapor-liquid-solid (VLS) process but following a new multiple nucleation growth model. The characterizations show that the obtained superstructures are composed of uniform single-crystalline ZnTe. The photoluminescence spectrum of the obtained multilayer ZnTe NW superstructures exhibits strong free exciton emission peak and relatively weak line, indicating that the layers are of high quality, which may have potential applications in nanodevices [74].

Kume et al. (2007) have investigated the homoepitaxial growth of ZnTe on the (100)-oriented ZnTe substrate by horizontal metalorganic vapor phase epitaxial (MOVPE) system at different reactor pressures using dimethylzinc and diethyl-telluride as source materials. The growth rate of ZnTe layers increases with increasing reactor pressure and becomes saturated eventually. The longitudinal optical phonon mode of ZnTe and a strong free exciton emission are clearly observed for all samples, indicating the ZnTe layers are of good crystal quality [75].

Zhang et al. (2008) presented to synthesis nanometer-sized ZnTe by precursor-reduction method. Zinc blende ZnTe nanocrystals growth in three different shapes under various conditions: quasi-spheres, tetrahedrons, and nanorods, have been observed. It is believed that the crystal growth of ZnTe is the rate-controlling step when superhydride was employed at 250°C, resulting in quasi-spherical ZnTe nanocrystals. Replacement of superhydride with oleylamine alters the precursor-reduction step as the rate-controlling step, giving tetrahedral ZnTe nanocrystals. At low temperature (150°C) and in the presence of superhydride and oley lamine, kinetic growth and/or surfactant-template dominate the process, causing an anisotropic crystal growth into ZnTe nanorods. ZnTe nanocrystals are typically surface-active with a similar crystal structure of CdSe. The present study provides a clue to understand the zinc blende-type nanocrystal growth mechanism in high-temperature colloidal system, and may lighten certain strategies of future nano materials processing, for example, the synthesis of one dimensional zinc blende-type semiconductors in solution phase [77].

Suriwong et al. [34] have succesfull synthesized cubic ZnTe nanocrystals. Zn and Te powders were mixted with 1:1 and 1.8:1 molar ratios of Zn:Te and using a 900W microwave plasma under 4.3±1 kPa argon absolute pressure. No such impurities were detected, when the experimental time length was optimized. Morphologies of molar ratio 1:1 and 1.8:1 were composed of 73.37 nm facet nanoparticles with different orientations and composed of a number of irregular nanoparticles in clusters, respectively.

2.9 Properties and synthesis of zinc oxide (ZnO)

Zinc Oxide (ZnO) is a key technological material, is a wide band-gap (3.37 eV) compound semiconductor that is suitable for short wavelength optoelectronic applications. The high exciton binding energy (60meV) in ZnO crystal can ensure efficient excitonic emission at room temperature and room temperature ultraviolet (UV) luminescence has been reported in disordered nanoparticles and thin films. In addition, the lack of a centre of symmetry in wurtzite, combined with large electromechanical coupling, results in strong piezoelectric and pyroelectric properties and the consequent use of ZnO in mechanical actuators and piezoelectric sensors. Furthermore, ZnO is a versatile functional material that has a diverse group of growth morphologies, such as nanocombs, nanorings, nanohelixes/nanosprings, nanobelts, nanowires and nanocages.

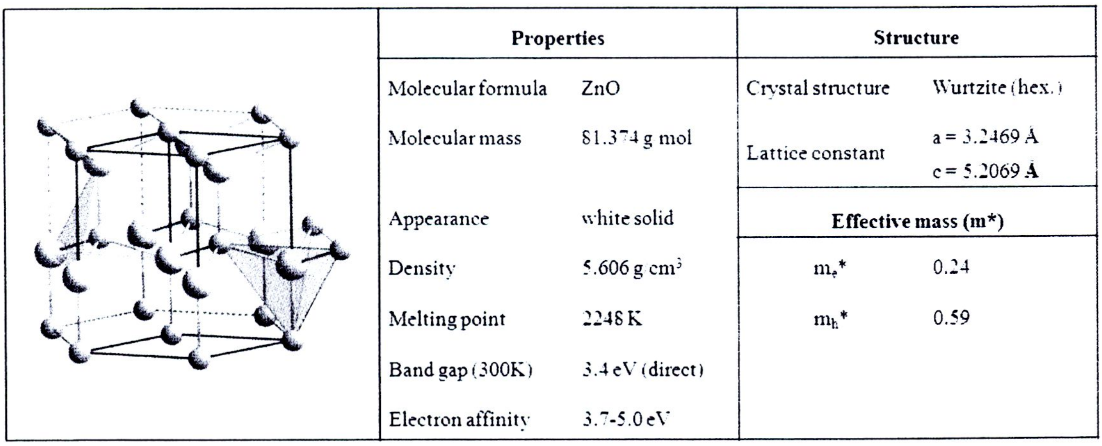

Properties		**Structure**	
Molecular formula	ZnO	Crystal structure	Wurtzite (hex.)
Molecular mass	81.374 g mol	Lattice constant	a = 3.2469 Å c = 5.2069 Å
Appearance	white solid	**Effective mass (m*)**	
Density	5.606 g cm^3	m_e*	0.24
Melting point	2248 K	m_h*	0.59
Band gap (300K)	3.4 eV (direct)		
Electron affinity	3.7-5.0 eV		

Figure 2.26 The properties and structure of ZnO (wurtzite) [70]